PLOS PATHOGENS

RESEARCH ARTICLE

Zika virus infects pericytes in the choroid plexus and enters the central nervous system through the blood-cerebrospinal fluid barrier

Jihye Kim[1], Brian Alejandro[1], Michal Hetman[2], Eyas M. Hattab[3], Joshua Joiner[4], Horst Schroten[5], Hiroshi Ishikawa[6], Dong-Hoon Chung[1,7]*

1 Department of Microbiology and Immunology, School of Medicine, University of Louisville, Kentucky, United States of America, **2** Department of Neurological Surgery, School of Medicine, University of Louisville, Kentucky, United States of America, **3** Department of Pathology and Laboratory Medicine, University of Louisville, Louisville, Kentucky, United States of America, **4** Centre College, Danville, Kentucky, United States of America, **5** Department of Pediatrics, Pediatric Infectious Diseases, Medical Faculty Mannheim, Heidelberg University, Mannheim, Germany, **6** Laboratory of Clinical Regenerative Medicine, Department of Neurosurgery, Faculty of Medicine, University of Tsukuba, Tsukuba, Ibaraki, Japan, **7** Center for Predictive Medicine, School of Medicine, University of Louisville, Kentucky, United States of America

* dhchun01@louisville.edu

Citation: Kim J, Alejandro B, Hetman M, Hattab EM, Joiner J, Schroten H, et al. (2020) Zika virus infects pericytes in the choroid plexus and enters the central nervous system through the blood-cerebrospinal fluid barrier. PLoS Pathog 16(5): e1008204. https://doi.org/10.1371/journal.ppat.1008204

Editor: Ted C. Pierson, NIH, UNITED STATES

Received: November 6, 2019

Accepted: April 7, 2020

Published: May 1, 2020

Data Availability Statement: All relevant data are within the manuscript and its Supporting Information files.

Funding: D.C and M.H were supported by the Collaborative Matching Grant Program from School of Medicine, University of Louisville. The funders had no role in study design, data collection and analysis, decision to publish, or preparation of the manuscript.

Competing interests: The authors have declared that no competing interests exist.

Abstract

Zika virus (ZIKV) can infect and cause microcephaly and Zika-associated neurological complications in the developing fetal and adult brains. In terms of pathogenesis, a critical question is how ZIKV overcomes the barriers separating the brain from the circulation and gains access to the central nervous system (CNS). Despite the importance of ZIKV pathogenesis, the route ZIKV utilizes to cross CNS barriers remains unclear. Here we show that in mouse models, ZIKV-infected cells initially appeared in the periventricular regions of the brain, including the choroid plexus and the meninges, prior to infection of the cortex. The appearance of ZIKV in cerebrospinal fluid (CSF) preceded infection of the brain parenchyma. Further the brain infection was significantly attenuated by neutralization of the virus in the CSF, indicating that ZIKV in the CSF at the early stage of infection might be responsible for establishing a lethal infection of the brain. We show that cells infected by ZIKV in the choroid plexus were pericytes. Using in vitro systems, we highlight the possibility that ZIKV crosses the blood-CSF barrier by disrupting the choroid plexus epithelial layer. Taken together, our results suggest that ZIKV might exploit the blood-CSF barrier rather than the blood-brain barrier to invade the CNS.

Author summary

Zika virus invades the human brains and causes Zika-associated neurological complications; however, the mechanism(s) by which Zika virus accesses the central nerves system remain unclear. Understanding of the cellular and molecular mechanisms will shed light on development of novel therapeutic and prophylactic targets for Zika virus and other neurotropic viruses. Here we use in vivo and in vitro models to understand how Zika

virus enters the brain. In mouse models, we found that Zika virus infects pericytes in the choroid plexus at very early stages of infection and neutralization of Zika virus in the cerebrospinal fluid significantly attenuates the brain infection. Further we show evidence that Zika virus can cross the epithelial cell layers in the choroid plexus from the blood side. Our research highlights that ZIKV invades the host brain by exploiting the blood-CSF barrier rather than the blood-brain barrier.

Introduction

The recent Zika virus (ZIKV) outbreaks in the Americas clearly revealed that ZIKV can cross various biological barriers and establish infections in body compartments that are separated from the general circulation. ZIKV is sexually transmittable over genital barriers[1], and ZIKV is often found in the eyes, which are protected from the circulation by the blood–retinal barrier[2,3]. Importantly, ZIKV invades the brain of both fetuses and adults. Successful invasion of the central nervous system (CNS) by ZIKV causes detrimental ZIKV-associated neurological complications such as microcephaly[4,5], encephalitis, myelitis, and meningoencephalitis in infants and adults [6–11]. In the context of infection of the CNS, which is separated from the circulation by a system of barriers, a critical question is how ZIKV gains access to the CNS from the circulation. Considering the fact that most nonneurological infections of ZIKV typically cause no to mild symptoms in humans, it is important to define the mechanism by which ZIKV crosses the barrier around the brain. Understanding of such mechanisms would shed light on novel therapeutic and prophylactic targets for ZIKV-induced neurological diseases.

The current speculation is that ZIKV crosses the BBB by productive infection of endothelial cells of the BBB[12,13]. It was previously shown that ZIKV infects primary human brain endothelial cells and is released from the basolateral side of the cell, indicating the potential release of virus from the endothelial cells into the cortex. However, no in vivo model studies have shown a clear understanding of how ZIKV invades the brain. Alternatively, an in vitro model using differentiated brain endothelial cells showed the potential of ZIKV to penetrate brain endothelial cell layers, which comprise the blood-brain barrier (BBB), without disrupting the structural integrity[14]. The infection of astrocytes, which are in close contact with endothelial cells, is known to be associated with breakdown of the BBB[15], which could provide a route to the brain. However, it remains unclear how ZIKV initially infects astrocytes or how ZIKV penetrates brain endothelial layers.

To gain insight into the mechanism by which ZIKV invades the brain, we employed interferon-deficient mouse models and analyzed the early events of brain infection. Using the models, we show that ZIKV infection in the brain starts from the infection of pericytes in the choroid plexus (ChP) followed by emergence of ZIKV in the cerebrospinal fluid (CSF). We also demonstrate that the ZIKV circulating in the CSF at the early stage of infection might be the source of the infection of the cortex by employing an intrathecal administration of neutralizing antibody prior to infection of the brain. Additionaly, using an in vitro primary human brain vascular pericyte model, we show that brain pericytes are indeed susceptible to ZIKV and ZIKV infection is dependent on AXL. A Transwell system of transformed human ChP epithelial cells (HIBCPP) demonstrated that ZIKV transport across the ChP epithelial layers could be a result of breakdown of the barrier by cellular factors from ZIKV-infected pericytes, without productive replication in ChP epithelial cells. Exposure of HIBCPP cells on Transwells to UV-irradiated conditioned media from ZIKV-infected HBVP resulted in the disruption of the barrier functions and the HIBCPP tight junctions. Our data collectively suggest that ZIKV

might invade the host brain by infection of pericytes followed by breach across the epithelial layers in the choroid plexus, the blood-CSF barrier.

Results

ZIKV Infection of the choroid plexus and the meninges preceded infection of the cortex in mouse models

Several studies using type-1 interferon receptor knockout mice have shown that when ZIKV is administered via subcutaneous, intraperitoneal, or intravenous routes, it establishes a robust brain infection in adult mice[16–18]. To understand the mechanism by which ZIKV gains access to the brain, we investigated an early stage of brain infection in type-1 interferon receptor knockout mice, B6(Cg)-Ifnar1tm1.2Ees/J (hereafter referred to as *Ifnar-/-*) with the PLCal_ZV strain of ZIKV. *Ifnar-/-* mice were infected with ZIKV subcutaneously, and the brains were harvested at 2, 3, and 4 days post infection (DPI). The brains were analyzed with in situ chromogenic RNA hybridization (hereafter, RNAScope assay) with a specific probe against the ZIKV genome. This method provided specific detection of ZIKV RNA in tissue mounted on slides. In our model, ZIKV-positive cells first appeared at 3 DPI in the choroid plexus (CP) and the meninges in the mouse brains (Fig 1). While particle-like ZIKV RNA stains were also detected within the brain capillaries (Fig 1 bi, gray arrowhead), no infected cells were detected in the capillaries of the cortex at 3 DPI. The CPs in all ventricles (i.e., lateral, third, and fourth ventricles) and the majority of meninges consistently showed strong positive signals for ZIKV in all samples (4 brains per timepoint) at 3 and 4 DPI (Fig 1 bii and cii, **black arrowhead or black arrow**). In the cortex, ZIKV-infected cells appeared for the first time at 4 DPI. At the early time points, the infection pattern in the cortex was focal and not evenly distributed throughout the entire brain area (Fig 1c, **black arrowheads)**. This infection pattern was remarkably different from the brains infected with Venezuelan equine encephalitis virus (strain TC-83 in AG129 mice, Fig 1d and S1 Fig) that showed widely distributed strong positive staining around the capillaries in the cortex as previously reported by others[19]. An independent experiment with cardiac perfusion prior to harvesting the brain showed identical findings, indicating the strong signals in the ChP and meninges were not from circulating blood cells (S2 Fig).

To confirm that the infection in the CP and meninges preceded that in the cortex, we compared the viral loads in these tissues using the quantitative real-time PCR (qRT-PCR) method (Fig 1e). *Ifnar-/-* mice infected with ZIKV as above were euthanized at 3 and 4 DPI and subjected to cardiac perfusion prior to the harvest of the brain to remove blood in the neurovascular systems. At 3 DPI, significant amounts of viral RNA were detected in the meninges and the CP but not in the cortex of the same brains. In the cortex, ZIKV appeared at 4 DPI. This result confirmed our findings with the chromogenic in situ RNA hybridization assay. The negative control group, cage mate $IFNAR^{+/-}$ mice infected with ZIKV, did not show any measurable amounts of viral RNA in all three tissues, confirming that spread to the brain might require IFNAR1 deficiency[15].

To understand if the infection of CP and meninges prior to the infection of the cortex is unique to this strain of ZIKV and mouse, we employed another mouse model, the AG129 model (IFN-α/β/γ receptor knockout strain), and other ZIKV isolates (DAK AR 41524 and PRVABC59) representing African and American lineages in addition to PLCal_ZV[4,17]. We found that the progress of ZIKV infection in the brains of AG129 mice was nearly identical to that of *ifnar-/-* mice. For the PLCal_ZV strain of ZIKV infection in AG129 mice, ZIKV-infected cells were found in the CP and the meninges at 4 DPI, and very little viral RNA staining was detected within the cerebral cortex region (S3 Fig). Robust infection in the cortex was

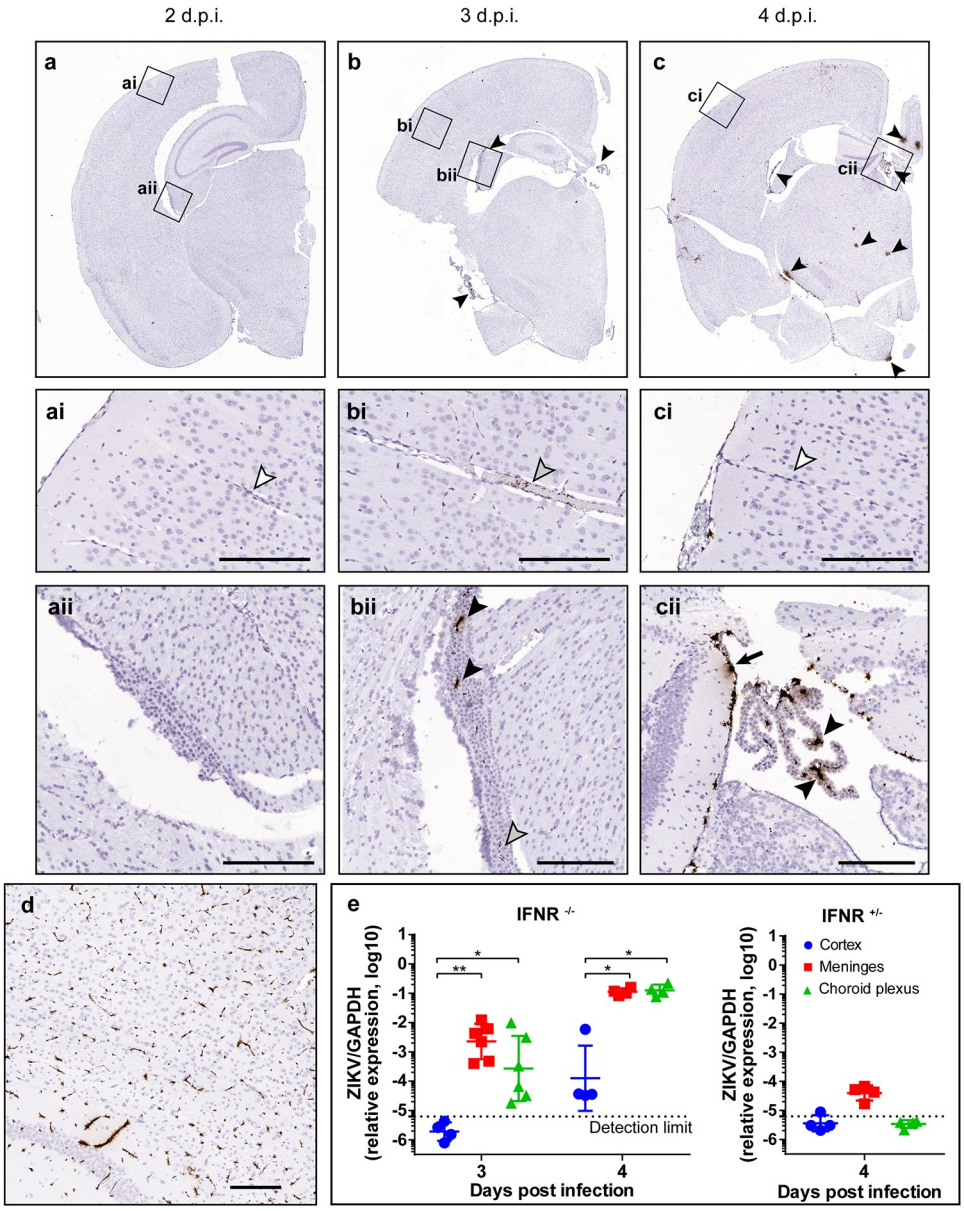

Fig 1. ZIKV infection of the brain in mice starts from the infection of the choroid plexuses and meninges. a-c, *Ifnar-/-* mice (n = 4 per time point) were subcutaneously infected with 1000 p.f.u. of ZIKV and euthanized at 2, 3, and 4 DPI. The brains were subjected to an in-situ RNA hybridization (RNAScope) assay with a probe detecting ZIKV RNAs. Positive signals for the target RNA are shown in dark brown, whereas the counterstaining with hematoxylin is shown in light blue. Images taken with a 20X objective were stitched with Hugin panorama image stitch software. Black, gray, and white arrowheads indicate virus-infected cells, virus, and the absence of ZIKV-specific staining, respectively. Detailed images of the areas outlined with a black box are shown in ai, bi, and ci (cortex and capillaries) and aii, bii, and cii (choroid plexus). Scale bars = 200 μm. **d**. AG129 mice (n = 3 per group, two experiments) were subcutaneously infected with 1000 p.f.u. of TC-83 and euthanized at 2 days post infection. The TC-83 vRNA was visualized in an RNAScope assay with a VEEV-specific probe. Scale bars = 200 μm. **e**, *Ifnar-/-* mice (left, n = 4–6/group) or IFNAR$^{+/-}$ mice (right, the cage mate n = 4) were infected with 1000 p.f.u. of ZIKV subcutaneously, and the brains were harvested at 3 and 4 DPI. The viral loads in the cortex (blue circles), meninges (red squares), and choroid plexuses (green triangles) were determined with a ZIKV-specific qRT-PCR assay and normalized to the expression of GAPDH mRNA in each sample. Data were analyzed by one-way ANOVA with Tukey's multiple comparison tests. * $P = 0.003$, ** $P = 0.0001$.

https://doi.org/10.1371/journal.ppat.1008204.g001

observed at 6 DPI. Again, little or no infection of the capillaries was found. These same findings–earlier infection of the meninges and CP than of the cortex–were observed for the DAK AR 41524 and PRVABC59 strains, indicating that infection of the CP and meninges is a common feature of ZIKV in these mouse models (S4 Fig).

Overall, these experiments revealed that ZIKV infects the choroid plexus and meninges in the brain, and the infection in these tissues precedes the infection of other regions in the brain.

ZIKV present in the CSF at the early stage is important for brain infection

To test whether ZIKV exploits the B-CSF barrier to enter into the CSF, we first examined the presence of virus in the CSF prior to infection of the cortex. After *Ifnar-/-* mice were infected with ZIKV subcutaneously, the CSF and serum were collected at 2, 3, and 4 DPI, and the viral loads were determined (Fig 2a). At 2 DPI, ZIKV was highly abundant in the serum with a median viral titer of 5.94×10^4 p.f.u./mL; however, no ZIKV was found in the CSF of the same animals. A significant level of ZIKV (median virus titer of 5.43×10^3 p.f.u./mL) was detected in the CSF at 3 DPI, at which time the CP was infected, but the cortex was not (Fig 1). While the viral load in the serum decreased at 4 DPI (1.56×10^4 p.f.u./mL) compared to 3 DPI (5.12×10^5 p.f.u./mL), the viral load in the CSF continued to increase to a titer of 1.11×10^4 p.f.u./mL at 4 DPI, which might be partially due to infection of the CP and cortex. This experiment clearly showed that the presence of ZIKV in the CSF precedes the infection of the cortex, indicating that ZIKV in the CSF might have directly originated from the blood across the B-CSF barrier.

Our results showed 1) active ZIKV replication in the meninges and the CP and 2) the presence of ZIKV in the CSF prior to active infection in the cortex. Together, these results suggest that ZIKV in the CSF at the early stage of infection is likely the result of infection of the CP and/or the meninges, not a consequence of the infection in the cortex. Hence, we hypothesized that ZIKV circulating in the CSF is responsible for CNS infection. To test this hypothesis, we employed intrathecal delivery of a ZIKV-neutralizing antibody in our ZIKV mouse model. *Ifnar-/-* mice were infected with ZIKV subcutaneously in the footpad as described above, and we administered either monoclonal anti-ZIKV IgM antibody (ZKA185 clone[20], mouse IgM isotype) or monoclonal anti-fluorescein IgM antibody (isotype control) intrathecally into the CSF through the cisterna magna at 2 or 3 DPI. The anti-ZIKV IgM antibody showed very strong neutralizing activity against ZIKV in vitro with a $PRNT_{50}$ of 1.3 ng/mL (S5 Fig). We chose the IgM isotype antibody over the IgG type to maximize availability in the CSF. The clearance rate of IgM in the CSF after intrathecal delivery is known to be approximately two-fold slower than that of IgG [21].

The effect of intrathecal delivery of anti-ZIKV IgM antibody was evaluated by comparing the viral loads in tissues and the clinical signs of disease at 6 DPI (Fig 2b, 2c and 2d). For this model, ZIKV-infected, untreated mice typically die or develop neurological symptoms thus meeting the euthanasia criteria at 7 DPI. Mice treated with anti-ZIKV IgM antibody showed a significantly lower brain viral load and clinical signs of disease than those of the isotype control group at 6 DPI. For example, when ZIKV-infected mice were treated with the antibodies at 3 DPI, the mean brain titers of the isotype control and anti-ZIKV IgM treated group were 3.27×10^8 p.f.u./g and 3.28×10^6 p.f.u./g brain tissue, respectively ($p<0.005$, Student's t-test). We also confirmed such a difference using the RNAScope assay with brain sections (Fig 2c). Similarly, the group treated with anti-ZIKV IgM showed much milder clinical signs of disease compared to those of the isotype control group at 6 DPI (Fig 2d). Viral loads of peripheral tissues (e.g., serum and spleen) showed no significant or little difference between the groups compared to those of the brain, indicating that the primary effect of antibody treatment was on the infection

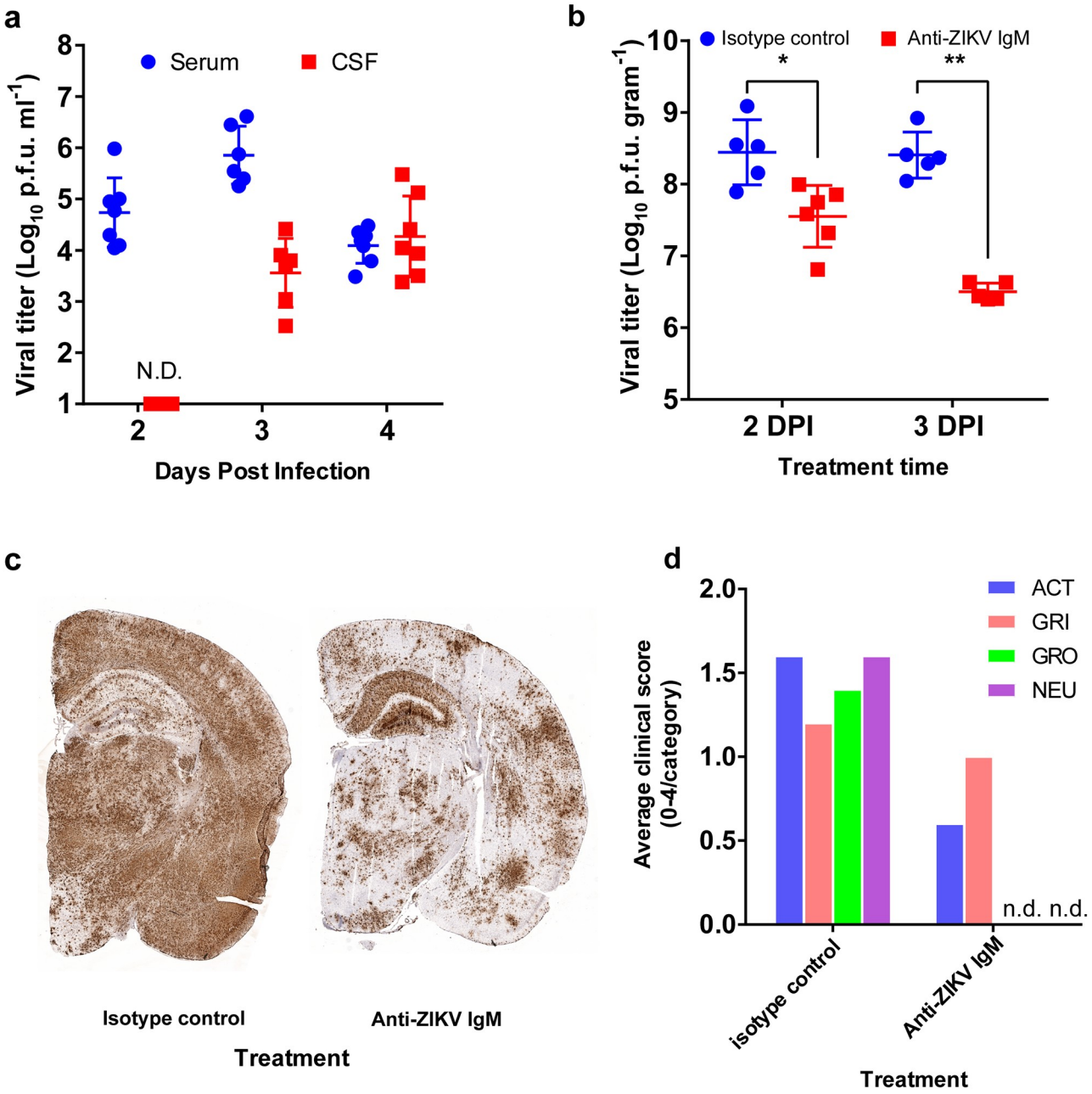

Fig 2. ZIKV in the CSF is critical to brain infection. a, *Ifnar*-/- mice (n = 6–8/time point from two independent experiments) were infected with ZIKV at the footpad as above. The serum and CSF were harvested at 2,3 and 4 DPI as described in the Methods section. The virus titers in the serum (blue circles) and in the CSF (red squares) were measured with a standard focus-forming assay in Vero 76 cells. **b-d**, Anti-ZIKV IgM or isotype control IgM was administered intrathecally to ZIKV-infected mice at 2 or 3 DPI (n = 6 per group per time point from two independent experiments). The brains were harvested at 6 DPI. **b**. The viral loads in the right hemisphere of the brains from the isotype control group (anti-fluorescein IgM, blue circles) and Anti-ZIKV IgM (red squares) were determined. **c**. A representative image of the RNAScope assay for the left hemisphere of the brains (n = 4 per group). **d**. Clinical scores (0 to 4, normal to severe) of the tested mice at 6 DPI. NEU: neurological symptoms; GRO: grooming; GRI: grimace scale; Act: Activity. n.d.: Not detected.

https://doi.org/10.1371/journal.ppat.1008204.g002

in the brain (S6 Fig). Intraperitoneal injection of the same antibody did not attenuate viral infection in the brain (S6 Fig). The observed attenuated brain infection by neutralization of the virus in the CSF demonstrated that ZIKV in the CSF at the early stage of infection might be responsible for establishing a lethal infection of the brain.

ZIKV infects pericytes, not endothelial cells in the CP

The strong ZIKV RNA signal in the CP and the unique biology of the CP led us to further investigate the CP as the ZIKV target tissue for brain invasion. The CP is a highly vascularized, specialized tissue located in the brain ventricles. The CP consists of a central stroma covered by two epithelial layers: the polarized CP epithelium facing the stroma at the basolateral side and the CSF at the apical side. Primary function of the CP is the production of CSF by transporting water and biomolecules between the blood and the CSF[5,22]. The production of CSF by the CP is mainly achieved by three cell types: 1) fenestrated endothelial cells that form capillaries, 2) pericytes, which are in direct contact with the endothelial cells and are responsible for regulating permeability, cerebrospinal blood flow, angiogenesis, clearance of debris, neuroinflammation, and stem cell activity[23–25], and 3) CP epithelial cells, which serve as the selective barrier between the blood and the CSF[22,26,27]. The tight junctions between the CP epithelial cells limit the paracellular diffusion of molecules across the barrier, and the transport of molecules is selectively achieved by transcytosis in CP epithelial cells [28,29]. Interestingly, unlike the blood vessels that comprise the blood-brain barrier in the parenchyma, the blood vessels in the choroid plexus are highly fenestrated and leaky, which can be an ideal milieu for infectious agents to easily spread into the tissue from the circulatory system[30,31].

We sought to define the cell type that initiates ZIKV brain infection in the CP. To understand the characteristics of ZIKV-infected cells in the CP, we employed confocal microscopy of whole-mount CP tissues. Consistent with the time course histochemistry results (Fig 1), we observed that ZIKV envelope(E)-positive cells were found in the choroid plexus (Fig 3). No endothelial cells (CD31+) showed positive staining for ZIKV; rather, ZIKV-infected cells were always in close contact with endothelial cells. High-resolution images showed that ZIKV-positive signals were always found in perivascular cells attached to capillaries or connecting two capillaries **(as shown in** Fig 3ai and 3b, **white arrowhead).** A three-dimensional reconstitution analysis showed that the ZIKV-infected cells are tightly associated with the endothelial cells (S7 Fig).

We confirmed this finding using secondary reagents: FITC-labeled *Griffonia simplicifolia* (Bandeiraea) isolectin B4 (IB4) and CPs isolated from ZIKV-infected AG129. IB4 is a lectin that can bind the basement membrane of capillaries or macrophages[32]. The CPs from ZIKV-infected AG129 mice also showed ZIKV E-positive cells located near endothelial cells throughout the entire CP (Fig 3c), which confirmed that ZIKV-positive cells were not endothelial cells but were in proximity of the capillaries in the CP.

Furthermore, we sought to determine the specific cell type that was infected by ZIKV in the CP. First, we confirmed that ZIKV-positive cells are not located in the CP epithelial cell layers (Fig 4a). CP epithelial cells are connected to each other with tight junction proteins at the apical and basolateral sides of the CP. Immunofluorescence microscopy using anti-TTR (i.e., transthyretin, a CP epithelial cell marker) antibody[33,34] showed that ZIKV-positive cells were located in the CP stroma space between the CP epithelial layers, not within the epithelial layers. This finding is different from what has been shown in a mouse model of chikungunya virus infection, where the CP epithelial cells were infected[35].

Based on the morphology and the location of the ZIKV-infected cells within the CP (Figs 3b and 4a), we hypothesized that the ZIKV-infected cells are pericytes. Pericytes are in direct contact with endothelial cells and continuously communicate with endothelial and other cells via secretory cytokines[36,37]. Brain vascular pericytes are responsible for regulating BBB permeability, cerebrospinal blood flow, angiogenesis, clearance of debris, neuroinflammation, and stem cell activity[23–25]. To test this hypothesis, we employed confocal fluorescence

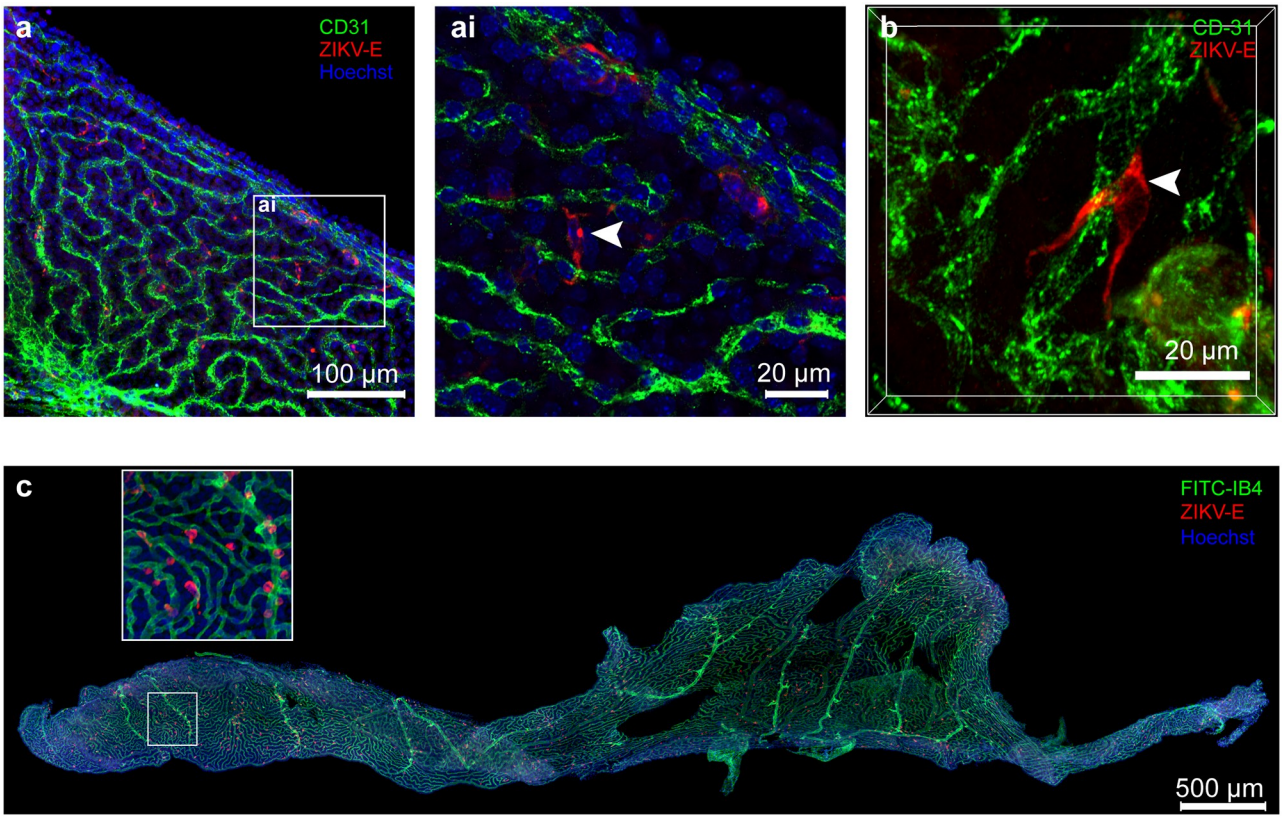

Fig 3. ZIKV-infected cells in the choroid plexus are tightly associated with endothelial cells. a, The lateral choroid plexuses from ZIKV-infected *Ifnar-/-* mice (n = 4 per time point) were harvested at 4 DPI and subjected to whole mount IFA assay. The whole tissue was stained with anti-CD31 antibody (endothelial cells, green), hu-4G2 (ZIKV envelope, red), and Hoechst 33342 (nuclei, blue) and then mounted for evaluation by confocal microscopy Scale bar = 100 μm. **ai**, A higher resolution image of the inset area of Fig **3 a**. Scale bars = 20 μm. **b**, A representative image of ZIKV-infected cells tightly connected with endothelial cells. Scale bars = 20 μm. **c**, The lateral choroid plexus of AG129 mice infected with ZIKV (1000 p.f.u. at 4 DPI) were stained with FITC-IB4 (endothelial layer, green), hu-4G2 (ZIKV envelope, red), and Hoechst 33342 (nuclei, blue). A total of 74 images taken with a 20X objective were stitched together with Hugin image stitch software. Scale bar = 500 μm.

https://doi.org/10.1371/journal.ppat.1008204.g003

microscopy of whole-mount CPs (Fig 4b) with an antibody against platelet-derived growth factor receptor beta (PDGFβR), a marker for pericytes [24,38,39]. The ZIKV-positive cells in the CP showed positive staining for PDGFβR (S8 Fig) and were found on the outer side of capillaries, indicating that the ZIKV-infected cells were indeed pericytes. A quantitative analysis demonstrated that 5 ~ 10% of total choroid plexus stromal cells stained positively for ZIKV at 4 dpi; furthermore, more than 90% of ZIKV E-positive cells were positive for PDGFβR (Fig 4c and 4d). Colocalization of ZIKV E protein and PDGFβR were not apparent within the double-positive cells (S8 Fig). No difference in the percentage of PDGFβR-positive cells in the stroma between mock and ZIKV-infected group was noticed (S8 Fig).

We also confirmed the replication of ZIKV in CP pericytes by using transmission electron microscopy (TEM) of ZIKV-infected CP (Fig 4e and 4f). Electron-dense particles with morphological characteristics typical of the nucleocapsid of flaviviruses were found on the surface of a vesicle in a cell adjacent to an endothelial cell on a CP capillary. The size of the particles was 28.2 ± 2.2 nm (mean and standard deviation from measurements of 28 particles), which is consistent with the size of immature ZIKV nucleocapsid cores previously determined by others[40]. Our results clearly showed that ZIKV targets pericytes not endothelial or epithelial cells in the CP.

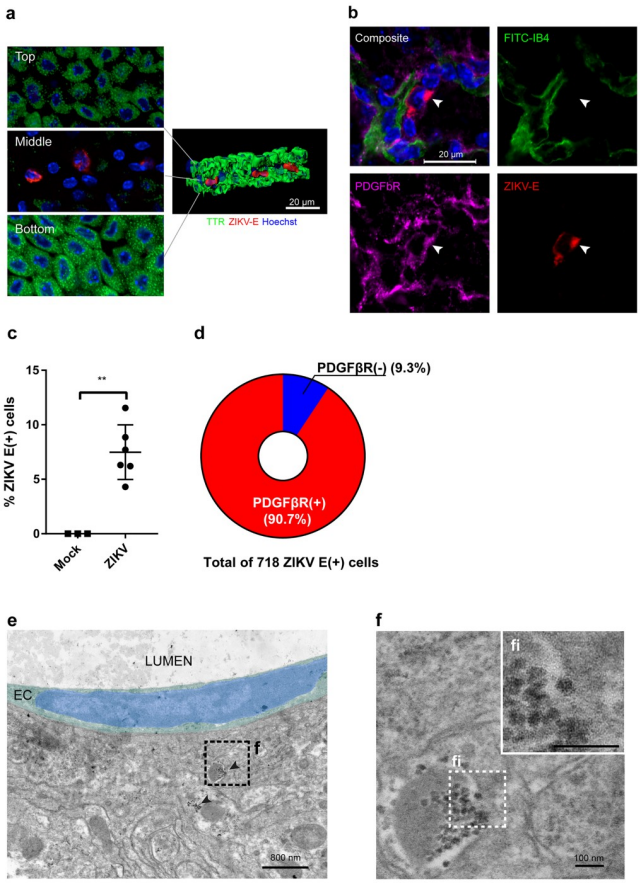

Fig 4. ZIKV infects pericytes in the choroid plexus. a-d, *Ifnar-/-* mice were infected with ZIKV as above, and the choroid plexuses were isolated at 4 DPI. **a**, Choroid plexuses were stained with antibodies against TTR (choroid plexus epithelial cell maker, green) and ZIKV-E protein (red). **left**: three layers of confocal images (labeled with Top, Middle, and Bottom) along the Z-axis. **right**: a three-dimensional reconstruction of the z-stacked image, highlighting the ZIKV-infected cells in the stroma layer of the choroid plexus. The top, middle, and bottom layers showed TTR +/ZIKV-, TTR-/ZIKV+, and TTR+/ZIKV-, respectively. A representative image is shown. **b**, Choroid plexuses were costained with FITC-IB4 for capillaries (green), anti-PDGFβR antibody for pericytes (purple), and anti-ZIKV-E antibody for the Zika envelope protein (red). Nuclei were stained with Hoechst 3342 stain (blue). The ZIKV-E signal colocalized with PDGFβR. For **a** and **b**, scale bars = 20 μm. **c-d**, ChP (n = 6, two from three mice) were harvested following cardiac perfusion and stained with anti-PDGFβR antibody for pericytes, anti-ZIKV-E antibody for the Zika envelope protein, and Hoechst 33342 for nuclei. (See S8 Fig for detail). The percentage of ZIKV-infected cells in the total ChP stromal cells(c) and PDGFβR (+) populations in the ZIKV (+) cells (d) were enumerated by using Imaris image analysis software. Each symbol represents an individual choroid plexus** $P < 0.01$ (Student's t-test). **e**, An electron micrograph showing a pericyte infected with ZIKV on a choroid plexus capillary. Pseudocolors (green and blue) indicate the cytoplasm and the nucleus, respectively, of a choroid plexus endothelial cell (EC) facing the lumen of a capillary (LUMEN). Patches of electron-dense particles (arrowheads) were found in a pericyte next to the EC. **f**, A higher magnification of the image from **e** shows that the particles have characteristics typical of flavivirus nucleocapsids. **fi**, A higher magnification image of the inset area of Fig **e**, Scale bars: 800 nm in **e** and 100 nm in **f and fi**.

https://doi.org/10.1371/journal.ppat.1008204.g004

Pericytes from mouse CP and human brains are susceptible to ZIKV infection

Next, we sought to model ZIKV infection of pericytes in vitro and examined the IFN dependence of ZIKV infection of pericytes. To test these models, we infected primary cultured mouse CP pericytes isolated from IFNAR$^{+/-}$ mice (Fig 5a) and primary human brain vascular pericytes (HBVPs) (Fig 5b) and tested the effect of IFN. The titers of progeny viruses produced

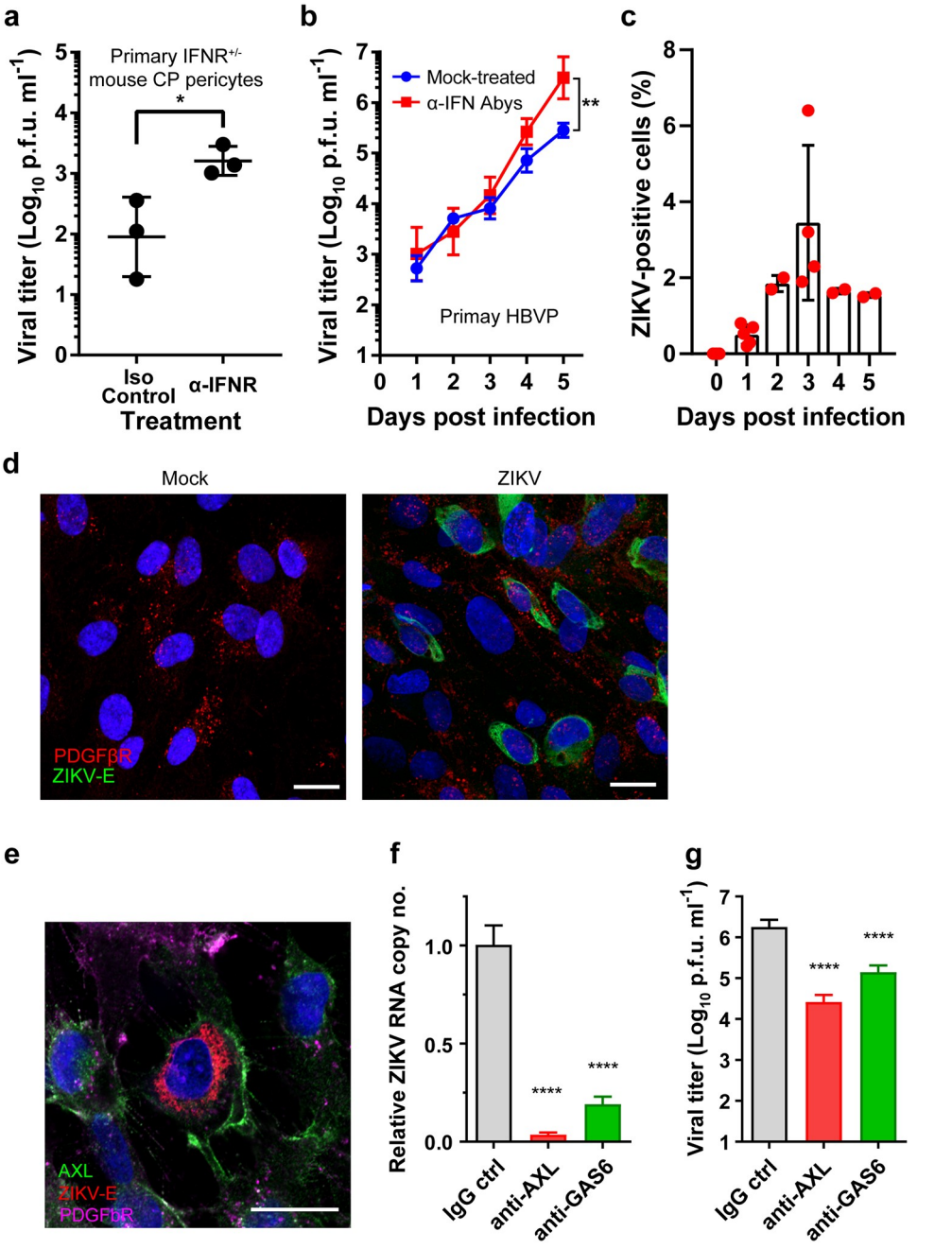

Fig 5. ZIKV infects human brain vascular pericytes in an AXL-dependent manner. a, ZIKV replication in primary pericytes from mouse choroid plexus ($IFNAR^{+/-}$). Cells (three independent wells) were infected with ZIKV, PLCal_ZV (MOI = 0.1) and grown in the presence of 5 μg/mL mouse anti-IFNAR-1 neutralizing antibody (clone MAR 5A3, -IFNAR) or isotype control antibody (clone MOPC-21). The cell culture supernatant was harvested at 5 DPI, and the virus titer was enumerated. * $P < 0.05$ (Student's t-test) **b**, Primary human brain vascular pericytes (five independent wells) were infected with ZIKV as in **a** and then incubated in the presence/absence of a human type 1 IFN neutralizing antibody mixture (-IFN Aby). The supernatants were harvested every 24 hours for five days, and the virus titers were enumerated with a virus titration assay. ** $P < 0.005$ (two-way ANOVA). **c**, Primary human brain vascular pericytes were infected with ZIKV and ZIKV-infected cells were enumerated by using FACS with anti ZIKV-E (clone 4G2). Each dot represents cells from single well. **d**, Mock- or ZIKV-infected HBVP were stained with antibodies against PDGFβR (red) and ZIKV-E protein (green). Two consecutive confocal layers were projected into a single layer with the Z-project function of ImageJ software (version 2.0.0). **e**, HBVP infected with ZIKV were stained with antibodies against AXL (green), PDGFβR (magenta) and ZIKV-E protein (red). Scale bars = 20 μm. **f** and **g**, HBVP were pre-treated with antibody for three hours then infected with ZIKV (m.o.i. = 1). Three days later, viral RNA (**f**) and progeny virus titers in the supernatants (**g**) were analyzed. **** $P < 0.001$ (one-way ANOVA).

https://doi.org/10.1371/journal.ppat.1008204.g005

from the cells were determined as proof of viral replication in the cells. We found that ZIKV was able to replicate and produce progeny virus in both cell types, indicating that pericytes are indeed susceptible to ZIKV infection. The mouse CP pericytes produced a low titer of progeny viruses in the absence of neutralizing antibody (NAb) against mouse type 1 interferon receptor (IFNAR-1). A slightly but significantly increased amount of progeny virus was generated in the presence of NAb against mouse IFNAR-1 (mean virus titers at 5 DPI of 162 and 1796 p.f.u./mL for isotype control and anti-IFNAR Ab, respectively, Fig 5a).

Because there are no commercially available human choroid plexus pericytes, we employed HBVP cells as our human pericyte model. HBVPs were more susceptible to ZIKV infection than mouse CP pericytes (Fig 5b), resulting in an increase in virus titer during the infection with a significant virus titer (mean titer of 2.93×10^5 p.f.u./mL at 5 DPI). ZIKV-infected HBVPs grown in the presence of antibody mixture of monoclonal and polyclonal antibodies directed against human Type 1 Interferons (IFNs) and Type 1 Receptor Subunit 2 (IFNAR2) produced an even higher amount of progeny virus (mean virus titer of 4.11×10^6 p.f.u./mL). Interestingly, not all HBVPs were susceptible to ZIKV. Only small fractions of HBVPs, approximately 1 to 3.5% compared to the total number of cells at its peak at 3 DPI, were positive for ZIKV (Fig 5c). These ZIKV-positive cells were positive for PDGFβR, a pericyte marker (Fig 5d). Our results clearly showed that mouse CP pericytes and human brain pericytes are susceptible to ZIKV infection and that the type 1 IFN system plays a limited role in controlling ZIKV replication in these cells.

AXL is a key factor for a productive infection of ZIKV in brain pericytes

TAM (TYRO3, AXL, MER) receptor tyrosine kinases are known important host factors that determine susceptibility to ZIKV as a cellular receptor for viral entry and/or an attenuator of innate antiviral response[41]. Notably, AXL receptor tyrosine kinase (AXL) is known to be important for efficient infection of human endothelial cells, skin cells, Sertoli cells, astrocytes, and brain glial cells [42–45]. However, some evidence indicates that the dependency of ZIKV on TAM receptors for infection might be cell-type or model specific (e.g., IFN dependency) [46,47]. Here we assessed if the AXL protein plays a role in the productive infection of pericytes. First, we confirmed that ZIKV-infected HBVP (i.e., ZIKV E and PDGFβR-positive) stained positively for AXL (Fig 5e). We also detected a significant AXL expression level in HBVP (see Fig 6f). Next, to understand the functional role of AXL in ZIKV infection, we examined the effect of blocking of AXL and growth arrest specific gene-6 (GAS6), ligand for AXL, on ZIKV replication in HBVP. A pretreatment of HBVP with anti-AXL or anti-GAS6 antibodies resulted in greater than 96% or 80% reduction, respectively, in viral replication measured by qRT-PCR (Fig 5f) of intracellular viral RNA, as well as a reduction in progeny viral titers (Fig 5g). Overall, our data clearly indicate that ZIKV-infection of HBVP is dependent on AXL and GAS6.

An in vitro blood-cerebrospinal fluid (B-CSF) barrier model recapitulates ZIKV entry into the CSF side

Then, we tested whether the tight junctions between CP epithelial cells were breached by the infection of the pericytes, which would allow virus to cross the B-CSF barrier and enter into the CSF. First, we employed a confocal microscopy assay for ZO-1 (zonula occluden-1, a tight junction-associated protein) to observe changes in tight junctions in whole-mount CP tissue from ZIKV-infected mice. We found that tight junctions are rather intact; no destruction of ZO-1 junctions were identified in the ZIKV-infected CP (Fig 5a).

To recapitulate the entry of ZIKV into the CSF through the B-CSF barrier, we developed an in vitro model utilizing the human choroid plexus papilloma (HIBCPP) cell line[48] and

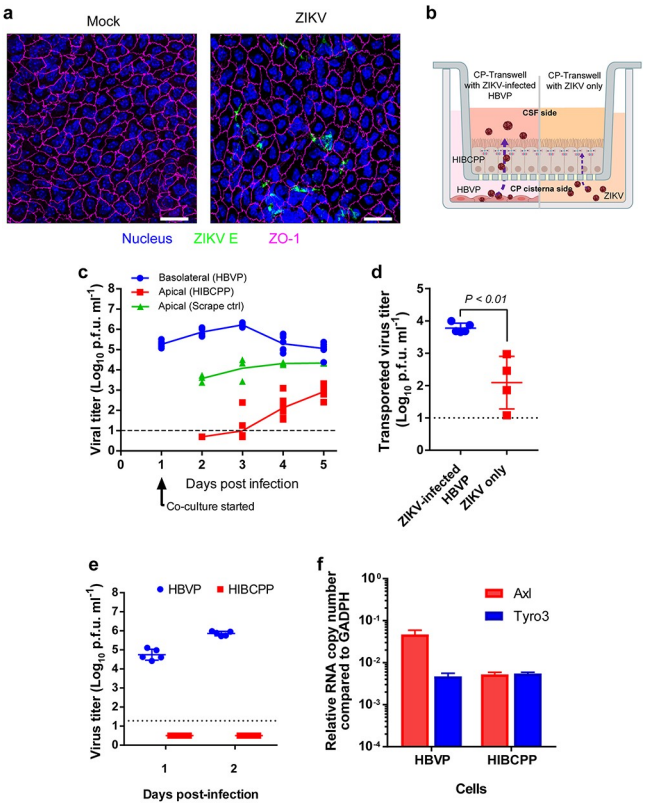

Fig 6. ZIKV crosses CP epithelial cell barriers. a, CPs isolated from ZIKV-infected mice were subjected to immunostaining in a whole-mount choroid plexus assay with antibodies against ZO-1 and ZIKV-E. The top and stroma cell layer was imaged with a Zeiss LSM 710 Duo/LIVE 5 confocal microscope along the Z-axis, and the maximum Z-project image was created with Imaris software. **b**, HIBCPP Transwell model. HIBCPP cells were grown and differentiated into a monolayer in Transwell inserts. Fully developed HIBCPP Transwell inserts (determined by TEER) were placed in wells with various testing conditions (e.g., primary human brain pericytes or conditioned media). **c**. Fully developed HIBCPP barriers grown in Transwell inserts (n = 3–5 per group) were basolaterally exposed to ZIKV-infected HBVP cells (starting at 1 DPI). As a leakage control, a scratch was made on the HIBCPP cells fully grown in Transwell inserts. Samples from the apical and basolateral chambers were harvested every 24 hours, and the virus titers were determined. **d**, Fully developed HIBCPP barriers grown in Transwell inserts (n = 4–5 per group) were basolaterally exposed to ZIKV-infected HBVP cells (3 d.p.i) or fresh media spiked with ZIKV (1.0×10^5 pfu/well/mL). Twenty-four hours later, the cell supernatant in the apical camber was harvested and the virus amount was enumerated. **e**, HBVP (blue circles) and HIBCPP (red squares) cells grown on 12-well plates were infected with ZIKV (m.o.i. = 0.1) and then incubated for two days. The virus titers in the supernatants were enumerated with a virus titration assay. **f**, Expression of Axl and Tyro3 in HBVP and HIBCPP was determined by using realtime q-PCR and normalized to endogenous GAPDH expression.

https://doi.org/10.1371/journal.ppat.1008204.g006

HBVP cells. HIBCPP is an established cell line derived from human CP epithelial cells and is known to form cellular barriers when it is grown and differentiated on Transwell membranes. HIBCPP cells grown and fully differentiated on Transwell membranes were exposed to ZIKV basolaterally by being placed in cell culture wells with HBVP cells that were infected with ZIKV for one day. Virus produced in the basolateral chambers and the apical chambers were harvested daily and enumerated. We found that a significant amount of ZIKV was transported to the apical chambers when the HIBCPP cell barrier was exposed to ZIKV-infected HBVP culture supernatant. Virus was detected in the apical chamber starting from two days post exposure and continuously increased (Fig 6c). Interestingly this transport was specific to HBVP culture because when the equal amount of ZIKV produced in Vero cells were provided in HVBP conditioned media, a significantly less amount of virus was transported to the apical

chamber (Fig 6d). When HIBCPP Transwells were exposed to HBVP cells which were infected with ZIKV for five days, an approximately 6.0 x 10^3 p.f.u./mL (n = 5) of virus was transported to the apical chamber for twenty-four hours. On the contrary, much less ZIKV was transported (a mean virus titer of 1.2 x 10^2 p.f.u./mL, n = 4) when ZIKV diluted in HBVP-conditioned media was used compared to when cells were cocultured with ZIKV-infected HBVPs. HIBCPP cells were resistant to ZIKV infection, which indicates that virus found in the apical chamber was not progeny virus produced in HIBCPP cells (Fig 6e). The expression of AXL and TYRO3, putative receptors for ZIKV entry, in HIBCPP was much lower than in brain pericytes (Fig 6f).

The integrity of the ChP barrier was compromised when exposed to ZIKV-infected pericytes

We sought to test if infected pericytes may play a role in promoting ZIKV to cross the B-CSF barrier. Fully developed HIBCPP Transwells were exposed to UV-treated conditioned media from mock- or ZIKV-infected HBVP and the barrier functions were measured over three days of exposure. Transwells exposed to conditioned medium from ZIKV-infected cells started losing the barrier significantly in transepithelial electrical resistance (TEER) (Fig 7a). We also detected a significantly higher degree of transport of FITC-dextran in the ZIKV-conditioned media group compared to the other groups after three days of exposure (Fig 7b). Confocal microscopy analysis showed a significantly higher number of cells with ZO-1 present in the cytosol, not in the cell-to-cell junctions, in the ZIKV-conditioned media treated group, indicating a loss of the barrier integrity (Fig 7c and 7d). This result could imply that cellular factors from ZIKV-infected pericytes might play a role in ZIKV transport across the ChP barrier.

Discussion

ZIKV is unique among flaviviruses with regards to its transmission and tissue distribution. Sexual transmission and infection of organs that are separated from the circulation (e.g., eyes, brain, fetus, and reproductive tract[6,49–51]) establish ZIKV as a unique flavivirus that can cross various biological barriers. Unlike other neuroinvasive flaviviruses such as West Nile virus or Japanese encephalitis virus, neuropathogenesis of ZIKV seems to be limited; however, non-human primate models and clinical studies still clearly demonstrated the neuroinvasive characteristic of ZIKV[8,52].

Here, we show that ZIKV might invade the brain from the circulation by exploiting the B-CSF barrier instead of the BBB. The BBB is the primary barrier that prevents most infectious agents from entering the brain. While many neurotropic viruses such as VEEV[19] are known to use the BBB as an entry route to the brain, the mechanism by which ZIKV enters the brain remains unclear. Some experimental findings highlighted the involvement of the breakdown of the BBB by ZIKV-infected astrocytes[53]; however, this may be a result of the brain infection rather than the brain entry mechanism for the following reasons: 1) later onset of BBB destruction than the initiation of brain infection (6 DPI compared to 3 DPI) and 2) the undefined origin of the virus that infected the astrocytes.

Our understanding of the role of CP in the context of brain infection is very limited; however, the CP exhibits many biological characteristics that can contribute to the entry of neurotropic viruses into the brain. Unlike the endothelial cells of the BBB, the CP endothelial cells are fenestrated and leaky (i.e., fenestrated blood capillaries with diaphragmed fenestrae) with fenestrae ranging between 60 and 80 nm in size[54]. Although some reports showed that the maximum size of molecules that can pass through the fenestrae may be smaller than the physical size of the fenestrae[55], the fenestrated endothelial cells of the CP could provide an ideal milieu for viruses to spread out of the blood and into the cisternae of the CP.

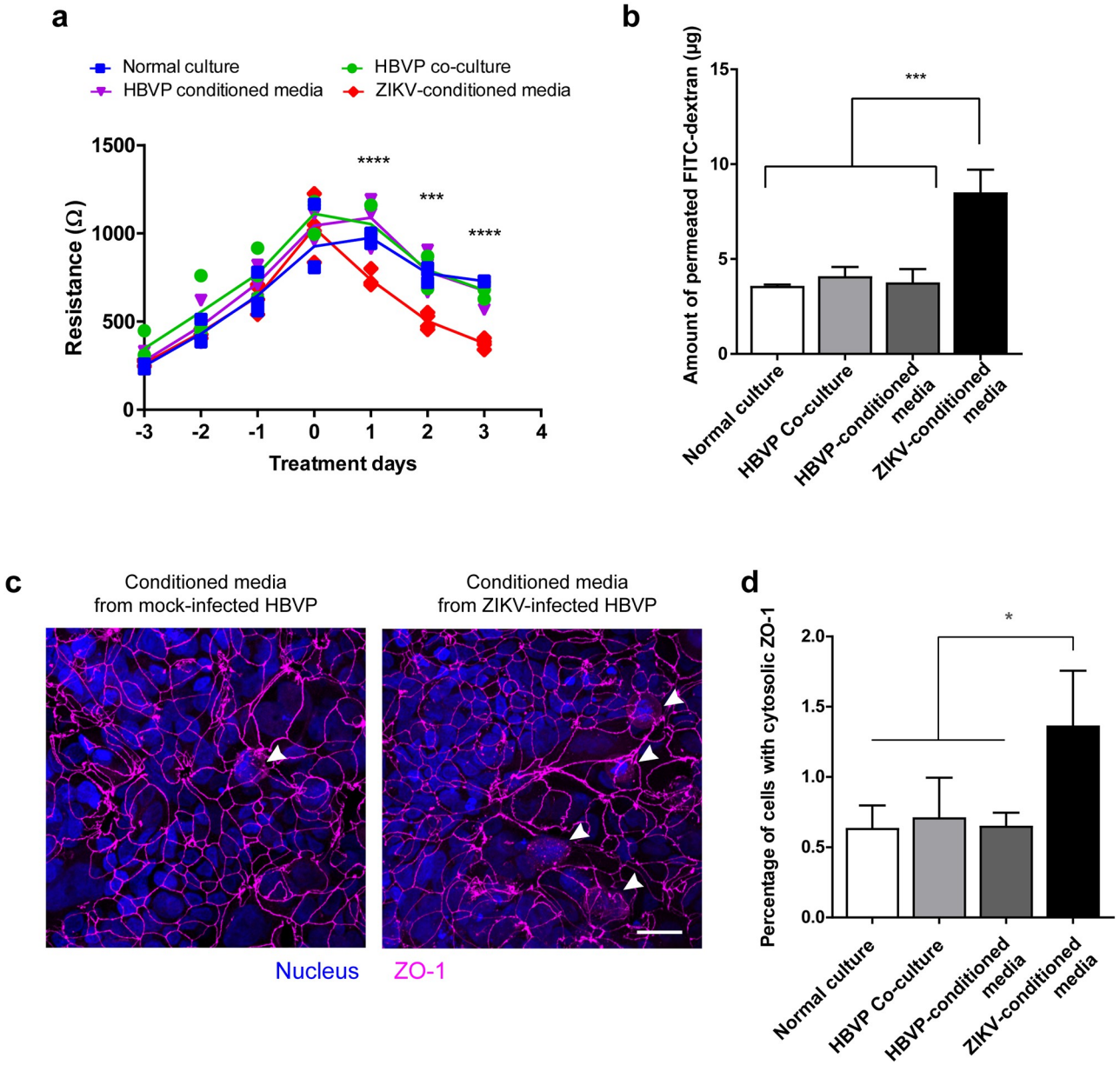

Fig 7. The barrier function of ChP epithelial cells is disrupted by ZIKV infection in pericytes. a-d, Fully developed HIBCPP barriers grown in Transwell inserts (n = 3–4 per group) were basolaterally treated with HBVP co-culture, UV-treated conditioned media from HBVP, or UV-treated cell supernatant from ZIKV-infected HBVP, and normal culture medium. The barrier functions were measured by TEER daily **(a),** and, at day 3 post treatment, FITC-dextran permeability (**b**) was measured. The transwells were stained with an anti-ZO-1 antibody (**c**, a representative image). Cells with cytosolic ZO-1 stain were counted (white arrow heads) and the percentage of the cells were analyzed (**d**). * P = 0.033 (one-way ANOVA); *** P = 0.0002, **** P < 0.0001 (two-way ANOVA).

https://doi.org/10.1371/journal.ppat.1008204.g007

Pericytes are in direct contact with endothelial cells; hence, viruses that have come out of the circulation through endothelial cells might directly contact nearby pericytes. Recent studies, which used fluorescent proteins under control of the NG2 (Cspg4) and PDGFRB promoters and single-cell sequencing of mouse brain cells, have identified several pericyte subpopulations in the brain, indicating a diversity of pericytes in both function and differentiation[56,57]. In addition, pericytes in the brain are known to differentiate into other cell types, such as

fibroblasts, indicating a substantial plasticity of pericytes[24,25]. While brain perivascular pericytes have been extensively studied at the BBB level[58,59], little is known about the biological functions of CP pericytes, especially the biological roles of CP pericytes with respect to viral invasion through the B-CSF barrier. Here, our study presents a novel finding that CP pericytes can be infected with ZIKV and might provide a local amplification site within the CP. Considering the variety of cytokines that are known to be secreted from pericytes[37,60], it would be important to understand other roles of ZIKV-infected CP pericytes in the viral invasion of the brain as well as in local inflammatory signals. Our data showing selective disruption of HIBCPP barrier by ZIKV-infected HBVP conditioned media suggest involvement of cellular cytokine or other factors for ZIKV CP barrier crossing. Still, a better approach to detect the breach of CP barrier in the mouse tissue samples is warranted.

The role of Axl in ZIKV infection has been studied extensively in mechanisms pertaining to: 1) cellular entry receptor and 2) attenuation of innate immune responses. ZIKV is known to bind to TAM receptors by using the ligands as a bridge, whereby TAM ligands (e.g., Gas6 or protein S) bind to phosphatidylserine exposed on virus particles and bridge virions to TAM receptors and the virus then utilizes the receptors as cellular receptors for entry, as well as attenuators of innate immune responses in the infected cells (i.e., the viral apoptotic mimicry mechanism)[44,45,61,62]. However, some evidence indicates that the dependency of ZIKV on TAM receptors for infection might be cell-type or model specific (e.g., IFN dependency) [46,47]. Our data clearly demonstrate that AXL is important for ZIKV infection in HBVP. A future study to understand to what extent the infection of pericytes is mediated via TAM receptors will be of great interest.

The IFNAR -/- mouse model, which is commonly used for ZIKV animal studies, allowed us to study the neuroinvasiveness of ZIKV easily with prominent replication in the brain; however, we also acknowledge the limitation of the model. Due to the lack of Type I interferon response in the model, cytokine responses may not reflect the actual mechanism in humans. In fact, Douglas et.al showed that infection of the CP by HSV-1 is dependent on the Type 1 interferon response; however, the infected cells in the CP seems to be CP epithelial cells not pericytes[63]. Future studies with recently developed models with the hSTAT2 knock-in mouse model [64] would be needed to validate our findings in the immunocompetent hosts.

With respect to the blood-brain interface, CP epithelial cells serve as a selective barrier and a professional transporter between the blood and the CSF[26]. The tight junctions between CP epithelial cells (e.g., zonula occludens) prevent paracellular diffusion. CP epithelial cells transport biological molecules across the epithelial barrier via transcytosis, which can be exploited by neurotropic viruses as a brain entry mechanism[28,65,66]. A very limited number of studies have been conducted with CP epithelial cells with respect to neuroinvasion. John Cunningham virus and chikungunya virus are known to infect CP epithelial cells in vitro[35,67]; however, to our knowledge, our study shows for the first time neurotropic viruses traversing the CP epithelial cell layers without active replication.

Our data demonstrate the importance of pericytes in ZIKV brain invasion via the B-CSF barrier, which was demonstrated as enhanced transport of ZIKV through the cells in our coculture model (Figs 6 and 7). It is of our great interest whether cytokines expressed in ZIKV-infected pericytes affect the integrity of the barrier. In addition, it is not clear that the infection of CP is unique to ZIKV or if other neurotropic flaviviruses may utilize the same mechanism. Future studies with other flavivuruses focusing on the early infection at the CP is of our great interest.

Overall, our study demonstrates a novel CNS invasion mechanism exploiting pericytes around fenestrated capillaries and epithelial cells in the B-CSF barrier of the CP by ZIKV. The ensemble of fenestrated capillaries, pericytes, and epithelial cell layer serves as a barrier and

transporter in other organs, such as the eye and the reproductive tract. Hence, our study might also shed light on the unique secretion and invasion profiles of ZIKV and new approaches to prevent the transmission of the virus.

Methods

Viruses

The ZIKV strains MR766 and PRVABC59 (GenBank: KX087101) were provided by Dr. Barbara Johnson at the CDC. The following reagents were obtained through BEI Resources, NIAID, NIH: ZIKV strains PLCal_ZV (Human/2013/Thailand; GenBank: KF993678) and DAK AR 41524 (Mosquito/1984/Senegal; GenBank: KX198134.2). ZIKV was amplified in Vero 76 cells (ATCC CRL-1587), and the titer was determined in Vero 76 cells with a standard methylcellulose overlay method described in a previously published paper[68]. VEEV TC-83 was obtained from USAMRIID (a gift from Dr. Connie Schmaljohn) and amplified in BHK-21 (ATCC CCL-10).

Antibodies

Mouse-4G2 (monoclonal antibody against anti-flavivirus group antigen, clone D1-4G2-4-15, ATCC), Hu-4G2 (recombinant monoclonal antibody of clone D1-4G2-4-15 with human IgG Fc produced in *Nicotiana tabacum*, a gift from Dr. Nobuyuki Matoba), anti-TTR (Abcam), anti-CD31 (Invitrogen), anti- PDGFβR (Abcam), anti-alpha smooth actin (Abcam), anti-Axl (R&D systems), FITC-isolectin B4 (Sigma Aldrich), Alexa Fluor 647-conjugated goat anti-rabbit IgG (Jackson ImmunoResearch), Alexa Fluor 549-conjugated goat anti-human IgG (Jackson ImmunoResearch), and Alexa Fluor 488-conjugated goat anti-rat IgG (H+L) (ThermoFisher) were used for the immunofluorescence assay. All antibodies were validated for their specificity using mock or isotype antibody controls.

Mouse IFNAR-1 neutralizing antibody (clone MAR 5A3) and isotype control (clone MOPC-21) were purchased from BioXcell. Anti-Axl (AF154), anti-GAS6 (AB885), and isotype control IgG (AB-108-C) were purchased from R&D systems. The human type 1 IFN neutralizing antibody mixture was purchased from PBL Assay Science. Anti-Zika mouse IgM antibody (Clone ZKA185) and an isotype control mouse IgM antibody (anti-fluorescein, clone 4-4-20) were obtained from Absolute Antibody.

Cells

Vero 76 cells (ATCC 1587) were obtained from ATCC and maintained in MEM-E with 10% FBS and L-glutamine. Primary human brain vascular pericytes (HBVPs) were obtained from ScienCell (Cat No. 1200) and maintained using the manufacturer's protocol and their pericyte culture media with 2% FBS, 1 x pericyte growth supplement, and 1 x penicillin and streptomycin.

Mouse choroid plexus pericytes (MCPPs) were isolated according to the protocol described by Boroujerdi et al.[69] with modifications. Choroid plexuses isolated from 4–5 mice at 5 weeks of $IFNAR^{+/-}$ were incubated in 1 mL of a papain/DNase I digestion solution (20 units of papain, 1 mM L-cysteine, and 0.5 mM EDTA in HBSS) at 37 ˚C for 50 min. After trituration of the choroid plexuses by 7 passages through a 19-gauge needle, followed by 7 passages through a 21-gauge needle, the cell mixture was mixed with the same volume of 22% BSA to neutralize the papain. Cells were harvested by centrifugation and suspended in 3 mL of endothelial cell growth medium (F12 medium with 10% FBS, 1x penicillin and streptomycin, 30 μg/mL endothelial cell growth supplement (Millipore), 2.5 μg/mL ascorbate, 1 x GlutaMax, and 40 μg/mL

heparin). Cells were plated on collagen type I-coated 35 mm dishes, and unattached cells were removed 2 hours after seeding. Pericytes were selected and cultured in pericyte growth medium (Pericytes Medium-mouse, Sciencell) for four passages prior to experiments. HIBCPP cells were obtained from Dr. Christian Schwerk's lab (Univ. of Heidelberg) and maintained according to a method published previously[48,70].

Mouse models and virus infection

Heterozygous Ifnar1tm1.2Ees mice (*Ifnar-/-*, interferon /β receptor deficient on the C57BL/6J background) were purchased from Jackson Laboratory (#028288). AG129 mice (interferon /β/ receptor deficient on the S129 background) were purchased from Marshall Bioresources. Mice were subsequently bred and housed at the University of Louisville. The genotypes of test mice were determined following the provider's protocol. Mice of both sexes between 4 and 6 weeks old were used for all experiments. Four- to six-week-old mice of both sexes were anesthetized under isoflurane and infected subcutaneously with 1000 p.f.u of virus (100% lethal in *Ifnar-/-* or in AG129 mice) diluted in PBS at the rear foot pad. Clinical scoring was performed as described in elsewhere [71]

In situ chromogenic RNA hybridization (i.e., RNAScope assay)

Mice were euthanized at the time points denoted in the experiments. The brains were harvested, and the left hemisphere of each brain was immediately placed in 10% buffered formalin and fixed for 24 to 48 hours followed by washing with 70% ethanol. The fixed brains were embedded in paraffin and sliced at a thickness of 5 μm and mounted on glass slides. Target RNA in the tissue sections was detected using RNAScope 2.5 Assay (Advanced Cell Diagnostics) and a specific probe according to manufacturer's protocol with a modification of 25 min of protease treatment instead of 30 min[72]. Stained tissues were counterstained with Gill's hematoxylin (American Master Tech Scientific), dehydrated, and mounted with glass coverslips using Cytoseal XYL (Fisher Scientific). Tissues were then visualized with a bright-field microscope. The image background was corrected with ImageJ as described elsewhere. (http://imagejdocu.tudor.lu/doku.php?id=howto:working:how_to_correct_background_illumination_in_brightfield_microscopy). High-resolution cross-section images were created using the Hugin Panorama photo stitching program (hugin.sourceforge.net) with small-field images for each image taken with a 10 × objective.

Determination of viral loads in the brain

Mice were infected subcutaneously with ZIKV strain PLCal_ZV. At 4 DPI, the mice were euthanized and transcardially perfused with 15 mL of PBS prior to the removal of the brains. The cerebral surface vasculature and associated meninges were harvested from the ventral and dorsal sides of the brains according to a protocol published by others[73]. Choroid plexus was isolated from all of the brain ventricles and pooled. Approximately 100 mg of cerebral cortex was harvested from the isocortex. Each tissue was homogenized in 0.5 mL of RNAzol RT (Molecular Research Center, Inc), and total RNA was isolated according to the manufacturer's protocol. The total RNA was subjected to reverse transcription with 200 U of Maxima H Minus Reverse Transcriptase and 2 μM of random hexamer in a total volume of 25 μL. qRT-PCR was performed in a multiplex format with 500 nM of ZIKV-specific primers and 250 nM of probes and a GAPDH-specific primer/probe set (4352339E, Applied Biosystems). The following ZIKV primer/probe sequences: Zika 1087 NW_fwd 5'-CCGCTGCCCAACACAAG-3' and Zika 1087 NW_rev 5'-CCACTAACGTTCTTTTGCAGACAT-3', and 5'/6-FAM/

AGCCTACCTT/ZEN/GACAAGCAATCAGACACTCAA/IABkFQ/3' were modified specific to the PLCal_ZV strain based on the sequences reported by Lanciotti et al.[74].

Immunostaining of whole-mount choroid plexus

Mice infected with 1000 p.f.u of ZIKV as described above were euthanized, and the brains were harvested immediately. The brains were rinsed twice in ice-cold HBSS, and the choroid plexuses were isolated from all ventricles (lateral, third, and fourth) under a stereoscope. The isolated choroid plexuses were incubated in HBSS with Mg^{2+} and Ca^{2+} containing 100 μg/mL DNase I (Akron Biotechnology) for 20 min at 37 ˚C followed by washing in PBS twice. The choroid plexuses were fixed with 4% paraformaldehyde in PBS for 20 min at 4 ˚C and washed twice in PBS with 0.1% Triton X-100. The fixed choroid plexuses were blocked with a blocking-permeabilization buffer (20% horse serum and 0.3% Triton-X100 in PBS) for two hours at 4 ˚C. For imaging, the fixed choroid plexuses were incubated overnight with antibodies for specific cell markers: anti-CD31 for endothelial cells, anti-ZIKV E for ZIKV, and anti-PDGFβR for pericytes, diluted with an antibody dilution buffer (2% goat serum and 0.1% Triton X-100 in PBS). Next, after two washes, the tissues were incubated with fluorophore-tagged secondary antibodies. For endothelial cell staining with FITC-isolectin B4, 10 μg/mL FITC-isolectin B4 (Sigma Aldrich) was added to the secondary antibody solution. These tissues were washed and further stained with Hoechst 33342 at a concentration of 1 μg/mL for 20 min. After mounting with ProLong Diamond antifade mount, immunofluorescent images were acquired using a Zeiss LSM 710Duo/Live5 confocal laser scanning fluorescence microscope. Images were processed using Imaris (Oxford Instruments) or FIJI (https://imagej.net/Fiji) software.

Collection of CSF and serum

CSF was collected according to the protocol by Nastasia et al.[75]. In brief, mice were anesthetized with an intraperitoneal injection of tribromoethanol (250 mg/kg), and the scalp was shaved. The dura of the cisterna magna was exposed by an incision under a stereoscope. CSF (1~5 μL per mouse) was harvested from the cisterna magna by a puncture of the dura with a capillary pipette (with an inner diameter of 50 μm). Blood contamination was determined by visual inspection of red blood cells in the CSF samples. CSF with blood contamination was excluded from further assays. After CSF collection, the blood was collected from the heart. The collected blood was incubated at room temperature for 20 min to allow clotting. The serum was harvested after centrifugation at 8,000 x g at 4 ˚C for 5 min. Blood-free CSF was suspended in 100 μL of complete media (MEM-E, 10% FBS, and 25 mM HEPES) and clarified by low-speed centrifugation for 5 min at room temperature. Collected samples were stored at -80 ˚C until use. Viral loads in the CSF and the serum were determined by following a standard methylcellulose overlay method as described previously[68].

Virus infection of primary HBVP and MCPP cells

Cells were seeded at a density of 50,000 cells/ well in 24-well plates coated with poly-L-lysine (for HBVPs) or collagen type-1 (for MCPPs) and incubated overnight prior to infection. Cells were infected with 10,000 p.f.u./well (~0.2 MOI) at 37 ˚C for one hour and washed with PBS twice to remove unbound virus. Cells were replenished with fresh media with anti-IFN neutralizing antibodies and incubated at 37 ˚C with 5% CO_2. At 1, 3, and 5 DPI, the cell culture supernatants were harvested, and the viral titers in the supernatants were determined in Vero 76 cells by following a standard methylcellulose overlay method as described above.

Immunostaining

For imaging HBVP cells were fixed in ice-cold methanol at room temperature for two minutes. For HIBCPP cells grown in Transwells, cells were fixed with 3% paraformaldehyde for 20 min. at 4 ˚C, Fixed cells were washed with PBS extensively, and then blocked with 5% normal goat serum and 0.1% Triton X-100 in PBS for one hour. Cells were then incubated at 4 ˚C overnight with primary antibodies for specific markers followed by fluorophore-conjugated secondary antibodies. All antibodies were diluted 1:400 in 1% BSA, 0.05% saponin in PBS. The glass slips were washed in PBS and further stained with Hoechst 33342 at a concentration of 1 μg/mL for 20 min. After mounting with ProLong Diamond antifade mount, immunofluorescent images were acquired using a Zeiss LSM 710Duo/Live5 confocal laser scanning fluorescence microscope. The proportion of infected cells were determined by image analysis. For each image, 16 fields-of-view taken with a 10 X objective were combined together and numbers of nuclei (i.e., total cell numbers) and ZIKV-E positive cells in each image were determined with Imaris software.

ZIKV-positive cell counting with flow cytometry

HBVP cells were seeded into T-25 cell culture flasks at a density of 600,000 cells/flask and were incubated for 2 days at 37 ˚C and 5% CO_2 prior to infection. The cells were then infected with ZIKV (0.1 MOI) by incubating with virus at 37 ˚C for 4 hours. After incubation, the cell supernatant was aspirated and replaced with fresh media. At the indicated timepoints (1, 2, 3, 4, or 5 days), the cells were detached from the culture surface by trypsinization with TrypLE Express (Gibco). After neutralization and trituration with pericyte culture media, the cells were passed through a 70 μm nylon filter (VWR International), washed twice with 1x PBS, and passed through a 70 μm filter again to ensure a single cell suspension. The cells were then fixed for 30 minutes at 4 ˚C in 4% paraformaldehyde and 0.1% saponin in 1x PBS. After washing of the cells with wash buffer (0.2% BSA, 0.1% saponin in 1x PBS) twice, the fixed cells were then stained with mouse-4G2 antibody (0.5 μg/mL in PBS with 1% BSA, 0.1% saponin) at room temperature for 1 hour. After incubation, the cells were washed with wash buffer once and then incubated with 1.5 μg/mL of Alexa Fluor 488-conjugated anti-mouse IgG in PBS with 1% BSA, 0.1% saponin for 1 hour at room temperature. Finally, the HBVP cells were washed three times with wash buffer and subjected to flow cytometry analysis. Flow cytometry analysis was performed using a BD LSRFortessa (BD Bioscience) flow cytometer with BD FACSDiva software (BD Bioscience). Forward scatter and side scatter voltages were optimized to place the population of interest on scale using an uninfected control sample. A histogram was created with the fluorescent intensity and cell counts. Cells with significantly higher fluorescent intensity than mock infected cells were considered ZIKV-positive cells. Further analysis was performed using FlowJo software (FlowJo).

AXL and GAS6 blockade

HBVP grown in 24-well plates were preincubated with 15 μg/ml anti-AXL antibody, 5μg/ml anti-GAS6 antibody, or goat polyclonal IgG control (n = 4 per group) for 3 hrs at 37˚C prior to infection. Cells were infected with ZIKV at an M.O.I of 1 for 4 hours and washed with PBS once. Cells were replenished with fresh media with half the concentration of antibodies and were incubated for two days. The total RNA was isolated from the cells and subjected to qRT-PCR for viral RNA quantitation. Viral titers in the supernatants were enumerated in a plaque assay as described above.

Expression of AXL and TYRO3 mRNA

Total RNA was isolated as described above. The expression of AXL and TYRO3 mRNA was determined by using the qRT-PCR with primer/probe sets with Hs01064444_m1 and Hs03986773_m1 (Thermofisher), respectively. The expression was normalized with expression of GAPDH mRNA.

Neutralization of ZIKV in the CSF

Mice (*Ifnar-/-*, n = 6 per group from three independent experiments) were infected with 1000 p.f.u. of ZIKV subcutaneously at the footpad. At 2 DPI, the mice were treated with anti-fluorescein mouse IgM (the isotype control group) or ZKA-185 mouse IgM (ZIKV neutralizing antibody group) via an intrathecal administration. For intrathecal administration, mice were anesthetized with an i.p. injection of a ketamine/xylazine mixture (100 and 5 mg/kg, respectively), and isoflurane was provided during the surgery. After the dura of the cisterna magna was exposed as described above in the "Collection of CSF and serum" section, 3 μL of antibody (1 mg/mL in PBS, 3 μg/mouse) was slowly administered into the cisterna magna cistern (3 μL/5 min) using a capillary pipette (tip size of 30 μm) controlled with a pneumatic microinjector (World Precision Instrument). After two min of resting after the capillary was retracted from the puncture, the incision was sutured, and the animals were returned to the cages. At 8 DPI, the animals were euthanized followed by cardiac perfusion with 15 mL of PBS. The right hemispheres of each brain were immediately placed in 10% buffered formalin and fixed for 24 to 48 hours for use in a ZIKV-RNAScope assay as described above. The remaining left hemispheres were homogenized in VIM at 10% (weight/volume) and then cleared by centrifugation. The virus titers and viral RNA copy numbers in the 10% brain homogenate were determined by the methylcellulose overlay method and qRT-PCR with a standard curve method.

Electron micrograph

Ifnar-/- mice were infected with ZIKV as above. At 4 DPI, mice were anesthetized with an intraperitoneal injection of tribromoethanol (250 mg/kg) and then transcardially perfused with 20 mL of ice-cold phosphate buffer saline to wash out the residual blood from the cerebral circulation. After perfusion with cold PBS, mice were perfused with 15 mL of fixative (2% paraformaldehyde, 2% glutaraldehyde in 0.1 M phosphate buffer, pH 7.4). The brains were harvested and then kept in the fixative. The choroid plexuses were isolated under a stereoscope and then fixed further at 4 ˚C for three days. After washing with phosphate buffer, the tissues were treated with 1% osmium tetroxide for two hours and then embedded with Durcupan resin. Sections were imaged with a transmission electron microscope (Hitachi HT7700).

Virus transport through Transwell inserts

To establish barriers on Transwell plates, HIBCPP cells (1.5×10^5) were seeded in the upper compartment of 24-well format Transwell inserts with a pore size of 3.0 μm and a density of $2 \times 10^6/cm^2$, coated with 2 μg mouse laminin. HIBCPP medium was replenished every two days. TEER was measured every two days and once it was confirmed to be > 600 Ω/insert; then, cells were further cultured in reduced FBS HIBCPP media with 2% FBS instead of 10% for one day and then used for experiments.

For co-culture of HBVP and HIBCPP cells, HBVP grown in 24-well plates overnight were infected with the ZIKV strain PLCAL_ZV at an MOI of 1 for 4 hours and then washed once with PBS before the addition of fresh culture media. At 1 DPI, Transwell inserts with fully developed HIBCPP barriers were placed in the well. Co-cultures were maintained by adding 1

mL HBVP medium to lower compartment and 0.4 mL 2% FBS HIBCPP medium to upper compartment. Supernatants from both compartments were collected from 1 DPI to 5 DPI.

Preparation of conditioned media

Cell culture supernatants from mock- or ZIKV-infected HBVP cells were harvested at 3–5 DPI then UV-treated for ten minutes (a total of 540 mJ/cm^2).

Fluorescein isothiocyanate (FITC)—Dextran permeability assay

In vitro Transwell permeability was measured with a modified previously published method [76]. FITC—dextran (Sigma Aldrich) was solubilized in 2% FBS HIBCPP medium to 1.5 mg/mL. The upper compartment of HIBCPP inserts was replenished with 0.4 mL of 2% FBS HIBCPP medium and 0.5mL of 1.5 mg/mL FITC-dextran was added to lower compartment. Inserts were incubated at 37˚C for 6 hours. The upper compartment supernatant from each insert was harvested, and 50 μL from each supernatant was added in triplicate to an opaque black bottom 96-well plate. FITC-dextran fluorescence was measured using a BioTek Synergy H4 plate reader with excitation/emission wavelengths of 485/530 nm. The amount of FITC-dextran in each sample was calculated using a standard curve.

Ethics statement

The animal experiments were carried out in strict accordance with the recommendations in the Guide for the Care and Use of Laboratory Animals of the National Institutes of Health. The animal experiments were conducted following an approved protocol (Protocol Number: 16533) by the University of Louisville Institutional Animal Care and Use Committee.

Supporting information

S1 Fig. VEEV TC-83 infects the brain at the level of BBB. The brains infected with Venezuelan equine encephalitis virus (strain TC-83) showed widely distributed strong positive staining around the capillaries in the cortex. Representative images of viral RNA staining with RNAScope assay of the brain cortex of TC-83 infected AG129 mice (n = 6 from two independent experiments). Images were taken with a 40 x objective. Cortex capillaries showed strong positive straining (dark brown) for viral RNA. Black and gray arrowheads indicate virus-infected cells and virus -specific staining, respectively.
(TIF)

S2 Fig. ZIKV infects cells in the choroid plexus in the brains of *Ifnar*-/- mice infected with ZIKV. *Ifnar*-/- mice infected with the PLCal_ZV strain (n = 3, 1000 p.f.u./mouse) were euthanized at 4 d.p.i. and cardiac perfusion was performed with 25 mL of PBS to remove the blood prior to tissue harvest. Brains were subjected to RNAScope assay to detect viral RNA. Representative images were shown here. Black arrowheads indicate virus-infected cells in the lateral ChP (**a**) and 4th ventricle ChP (**b**).
(TIF)

S3 Fig. ZIKV appears in the stroma area of the choroid plexus first in brains of AG129 mice infected with ZIKV. Brains from AG129 mice infected with PLCal_ZV (n = 3/timepoint, 1000 puf/mouse) were subjected to RNAScope assay to detect viral RNA. For **a**-**c**, representative images were shown from brains harvested at 2, 4, and 6 days post infection. Black arrowheads indicate virus-infected cells. Scale bars, 100 μm.
(TIF)

S4 Fig. Infection of the choroid plexus and meninges of the brain at the early stage of infection is a common feature of ZIKV brain infection. Representative images of the brains of AG129 mice infected with ZIKV strain DA KAR (**a**-**c**) and PRVABC59 (d-e) (n = 3 per group). The brains were harvested at 3 d.p.i. and were analyzed with RNAScope assay with a specific probe against the ZIKV.
(TIF)

S5 Fig. Plaque reduction neutralization activity of antibody used for in vivo neutralization. ZIKV-specific antibodies, clones ZKA 64 and ZKA 185, were serially diluted in cell growth media with HEPES (12.5 mM) and incubated with ZIKV strain PLCal_ZV (100 p.f.u./sample) for one hour at 37 ˚C. Vero 76 cells grown overnight in 12-well plates were infected with the antibody-virus mix and 5 days later viral plaques were developed by crystal violet staining. Anti-fluorescein mouse IgG and anti-fluorescein IgM were used as non-neutralizing antibody control (10 ng/mL).
(JPG)

S6 Fig. In vivo effect of ZIKV neutralizing antibody delivered via the intrathecal or intraperitoneal routes. a, Intrathecal delivery of neutralizing antibody did not affect viral growth in peripheral tissues as much as in the brain. Viral loads of the serum and the spleens of ZIKV-infected mice treated either with isotype control (blue circles) or with ant-ZIKV IgM (red squares) showed no significant (serum) or less significant difference (spleen) than for the brains (6 d.p.i, n = 5-6/group). **b**, Intraperitoneal delivery of neutralizing antibody did not show any difference in viral replication in tissues, including brain. Antibodies (n = 4-5/group, 3 μg/mouse which is the same dose used for intrathecal delivery) were administrated intraperitoneally at 3 d.p.i. and the mice were euthanized at 7 d.p.i. Viral loads were determined with 10% tissue homogenates. N.S. no significance by Student t-test $P > 0.05$.
(TIF)

S7 Fig. A reconstituted 3D model of a ZIKV-infected pericyte. A reconstructed 3-D image of Fig 3b. Images were acquired with a confocal laser scanning microscope and a three-dimensional image was reconstructed with the image analysis software Imaris using its surface modeling function. CD31 (green) and ZIKV-E (red) were used as markers for endothelial cells and ZIKV-infected cells. Scare bar, 20 μm.
(TIF)

S8 Fig. Colocalization of ZIKV and PDGFR-β cells in the choroid plexus of *Ifnar*-/- mice infected with ZIKV. Mock (**a**) or ZIKV (**b**)–infected mice were euthanized at 4 dpi and cardiac perfusion was performed and the choroid plexuses were harvested. The whole-mount choroid plexus tissues were stained with rabbit anti-PDGFR-β (green, Alexa 488-conjucated anti-rabbit IgG) and mAby hu-4G2 (red, Alexa594-conjugated anti-human IgG) antibodies. Images of the stroma layer of the CPs were taken with Zeiss LSM 710Duo/Live5 confocal laser scanning fluorescence microscope with a 40 x object. **c**. A representative image with a high magnification (63X objective). **d**. Comparison of number of PDGFR-β(+) cells PDGFR-β(+) cells were counted from three mock-infected and six ZIKV-infected mouse choroid plexuses. N.S., $P > 0.05$ with Student t-test.
(TIF)

Acknowledgments

We thank BEI Resource and Dr. Barbara at the CDC for providing ZIKV strains. We also thank Dr. Christian Schwerk for providing the HIBCPP cell line. We are grateful to Robert

Adcock, University of Louisville Center for Predictive Medicine Animal Core, University of Louisville EM Core, and Iowa State University Comparative Pathology lab for helpful technical support. We also thank Dr. David Magnuson for helpful comments and insights and Christine Yarberry, Gretchen Holz, and Dr. Yong-kyu Chu for establishing the assays. This research was supported by the Collaborative Matching Grant Program from School of Medicine, University of Louisville. All experiments involving animals and animal tissues were performed in accordance with protocols approved by the University of Louisville Institutional Animal Care and Use Committee.

Author Contributions

Conceptualization: Michal Hetman, Dong-Hoon Chung.

Data curation: Jihye Kim, Brian Alejandro, Eyas M. Hattab, Joshua Joiner, Dong-Hoon Chung.

Formal analysis: Jihye Kim, Brian Alejandro, Eyas M. Hattab, Dong-Hoon Chung.

Funding acquisition: Dong-Hoon Chung.

Investigation: Jihye Kim, Dong-Hoon Chung.

Methodology: Jihye Kim, Michal Hetman, Dong-Hoon Chung.

Project administration: Dong-Hoon Chung.

Resources: Horst Schroten, Hiroshi Ishikawa.

Supervision: Dong-Hoon Chung.

Visualization: Dong-Hoon Chung.

Writing – original draft: Dong-Hoon Chung.

Writing – review & editing: Jihye Kim, Brian Alejandro, Michal Hetman, Dong-Hoon Chung.

References

1. Yockey LJ, Varela L, Rakib T, Khoury-Hanold W, Fink SL, Stutz B, et al. Vaginal Exposure to Zika Virus during Pregnancy Leads to Fetal Brain Infection. Cell. 2016; 166: 1247–1256.e4. https://doi.org/10.1016/j.cell.2016.08.004 PMID: 27565347
2. Kodati S, Palmore TN, Spellman FA, Cunningham D, Weistrop B, Sen HN. Bilateral posterior uveitis associated with Zika virus infection. Lancet Lond Engl. 2017; 389: 125–126. https://doi.org/10.1016/S0140-6736(16)32518-1
3. Manangeeswaran M, Kielczewski JL, Sen HN, Xu BC, Ireland DerekDC, McWilliams IL, et al. ZIKA virus infection causes persistent chorioretinal lesions. Emerg Microbes Infect. 2018;7. https://doi.org/10.1038/s41426-017-0007-8 PMID: 29362446
4. Driggers RW, Ho C-Y, Korhonen EM, Kuivanen S, Jääskeläinen AJ, Smura T, et al. Zika Virus Infection with Prolonged Maternal Viremia and Fetal Brain Abnormalities. N Engl J Med. 2016; 374: 2142–2151. https://doi.org/10.1056/NEJMoa1601824 PMID: 27028667
5. Johansson MA, Mier-y-Teran-Romero L, Reefhuis J, Gilboa SM, Hills SL. Zika and the Risk of Microcephaly. N Engl J Med. 2016; 375: 1–4. https://doi.org/10.1056/NEJMp1605367 PMID: 27222919
6. Rozé B, Najioullah F, Signate A, Apetse K, Brouste Y, Gourgoudou S, et al. Zika virus detection in cerebrospinal fluid from two patients with encephalopathy, Martinique, February 2016. Eurosurveillance. 2016; 21. https://doi.org/10.2807/1560-7917.ES.2016.21.16.30205 PMID: 27123558
7. Carteaux G, Maquart M, Bedet A, Contou D, Brugières P, Fourati S, et al. Zika Virus Associated with Meningoencephalitis. N Engl J Med. 2016; 374: 1595–1596. https://doi.org/10.1056/NEJMc1602964 PMID: 26958738

8. Silva IRF da Frontera JA, de Filippis AMB, do Nascimento OJM. Neurologic Complications Associated With the Zika Virus in Brazilian Adults. JAMA Neurol. 2017 [cited 22 Sep 2017]. https://doi.org/10.1001/jamaneurol.2017.1703 PMID: 28806453

9. de Araújo TVB, Rodrigues LC, de A Ximenes RA, de B Miranda-Filho D, Montarroyos UR, de Melo APL, et al. Association between Zika virus infection and microcephaly in Brazil, January to May, 2016: preliminary report of a case-control study. Lancet Infect Dis. 2016; 16: 1356–1363. https://doi.org/10.1016/S1473-3099(16)30318-8 PMID: 27641777

10. Mehta R, Soares CN, Medialdea-Carrera R, Ellul M, da Silva MTT, Rosala-Hallas A, et al. The spectrum of neurological disease associated with Zika and chikungunya viruses in adults in Rio de Janeiro, Brazil: A case series. PLoS Negl Trop Dis. 2018; 12: e0006212. https://doi.org/10.1371/journal.pntd.0006212 PMID: 29432457

11. Mécharles S, Herrmann C, Poullain P, Tran T-H, Deschamps N, Mathon G, et al. Acute myelitis due to Zika virus infection. The Lancet. 2016; 387: 1481. https://doi.org/10.1016/S0140-6736(16)00644-9

12. Mladinich MC, Schwedes J, Mackow ER. Zika Virus Persistently Infects and Is Basolaterally Released from Primary Human Brain Microvascular Endothelial Cells. mBio. 2017; 8. https://doi.org/10.1128/mBio.00952-17 PMID: 28698279

13. Papa MP, Meuren LM, Coelho SVA, de O Lucas CG, Mustafá YM, Lemos Matassoli F, et al. Zika Virus Infects, Activates, and Crosses Brain Microvascular Endothelial Cells, without Barrier Disruption. Front Microbiol. 2017; 8. https://doi.org/10.3389/fmicb.2017.02557 PMID: 29312238

14. Alimonti JB, Ribecco-Lutkiewicz M, Sodja C, Jezierski A, Stanimirovic DB, Liu Q, et al. Zika virus crosses an in vitro human blood brain barrier model. Fluids Barriers CNS. 2018; 15. https://doi.org/10.1186/s12987-018-0100-y PMID: 29759080

15. Jurado KA, Yockey LJ, Wong PW, Lee S, Huttner AJ, Iwasaki A. Antiviral CD8 T cells induce Zika-virus-associated paralysis in mice. Nat Microbiol. 2018; 3: 141–147. https://doi.org/10.1038/s41564-017-0060-z PMID: 29158604

16. Aliota MT, Caine EA, Walker EC, Larkin KE, Camacho E, Osorio JE. Characterization of Lethal Zika Virus Infection in AG129 Mice. PLOS Negl Trop Dis. 2016; 10: e0004682. https://doi.org/10.1371/journal.pntd.0004682 PMID: 27093158

17. Lazear HM, Govero J, Smith AM, Platt DJ, Fernandez E, Miner JJ, et al. A Mouse Model of Zika Virus Pathogenesis. Cell Host Microbe. 2016; 19: 720–730. https://doi.org/10.1016/j.chom.2016.03.010 PMID: 27066744

18. Li C, Xu D, Ye Q, Hong S, Jiang Y, Liu X, et al. Zika Virus Disrupts Neural Progenitor Development and Leads to Microcephaly in Mice. Cell Stem Cell. 2016; 19: 120–126. https://doi.org/10.1016/j.stem.2016.04.017 PMID: 27179424

19. Cain MD, Salimi H, Gong Y, Yang L, Hamilton SL, Heffernan JR, et al. Virus entry and replication in the brain precedes blood-brain barrier disruption during intranasal alphavirus infection. J Neuroimmunol. 2017; 308: 118–130. https://doi.org/10.1016/j.jneuroim.2017.04.008 PMID: 28501330

20. Stettler K, Beltramello M, Espinosa DA, Graham V, Cassotta A, Bianchi S, et al. Specificity, cross-reactivity, and function of antibodies elicited by Zika virus infection. Science. 2016; 353: 823–826. https://doi.org/10.1126/science.aaf8505 PMID: 27417494

21. Bergman I, Burckart GJ, Pohl CR, Venkataramanan R, Barmada MA, Griffin JA, et al. Pharmacokinetics of IgG and IgM anti-ganglioside antibodies in rats and monkeys after intrathecal administration. J Pharmacol Exp Ther. 1998; 284: 111–115. PMID: 9435168

22. Benarroch EE. Choroid plexus–CSF system: Recent developments and clinical correlations. Neurology. 2016; 86: 286–296. https://doi.org/10.1212/WNL.0000000000002298 PMID: 26683646

23. Sweeney MD, Ayyadurai S, Zlokovic BV. Pericytes of the neurovascular unit: key functions and signaling pathways. Nat Neurosci. 2016; 19: 771–783. https://doi.org/10.1038/nn.4288 PMID: 27227366

24. Dore-Duffy P. Pericytes: Pluripotent Cells of the Blood Brain Barrier. Curr Pharm Des. 2008; 14: 1581–1593. https://doi.org/10.2174/138161208784705469 PMID: 18673199

25. Göritz C, Dias DO, Tomilin N, Barbacid M, Shupliakov O, Frisén J. A Pericyte Origin of Spinal Cord Scar Tissue. Science. 2011; 333: 238–242. https://doi.org/10.1126/science.1203165 PMID: 21737741

26. Wolburg H, Paulus W. Choroid plexus: biology and pathology. Acta Neuropathol (Berl). 2010; 119: 75–88. https://doi.org/10.1007/s00401-009-0627-8 PMID: 20033190

27. Zheng W, Perry DF, Nelson DL, Aposhian HV. Choroid plexus protects cerebrospinal fluid against toxic metals. FASEB J. 1991; 5: 2188–2193. https://doi.org/10.1096/fasebj.5.8.1850706 PMID: 1850706

28. Praetorius J, Damkier HH. Transport across the choroid plexus epithelium. Am J Physiol-Cell Physiol. 2017; 312: C673–C686. https://doi.org/10.1152/ajpcell.00041.2017 PMID: 28330845

29. Uriarte M, De Francesco PN, Fernandez G, Cabral A, Castrogiovanni D, Lalonde T, et al. Evidence Supporting a Role for the Blood-Cerebrospinal Fluid Barrier Transporting Circulating Ghrelin into the Brain. Mol Neurobiol. 2018. https://doi.org/10.1007/s12035-018-1362-8 PMID: 30276663

30. Johansson PA. The choroid plexuses and their impact on developmental neurogenesis. Front Neurosci. 2014; 8. https://doi.org/10.3389/fnins.2014.00340 PMID: 25386116

31. Saunders NR, Dreifuss J-J, Dziegielewska KM, Johansson PA, Habgood MD, Møllgård K, et al. The rights and wrongs of blood-brain barrier permeability studies: a walk through 100 years of history. Front Neurosci. 2014; 8. https://doi.org/10.3389/fnins.2014.00404 PMID: 25565938

32. Cheng J, Korte N, Nortley R, Sethi H, Tang Y, Attwell D. Targeting pericytes for therapeutic approaches to neurological disorders. Acta Neuropathol (Berl). 2018; 1–17. https://doi.org/10.1007/s00401-018-1893-0 PMID: 30097696

33. Janssen SF, van der Spek SJF, ten Brink JB, Essing AHW, Gorgels TGMF, van der Spek PJ, et al. Gene Expression and Functional Annotation of the Human and Mouse Choroid Plexus Epithelium. PLOS ONE. 2013; 8: e83345. https://doi.org/10.1371/journal.pone.0083345 PMID: 24391755

34. Lazarevic I, Engelhardt B. Modeling immune functions of the mouse blood–cerebrospinal fluid barrier in vitro: primary rather than immortalized mouse choroid plexus epithelial cells are suited to study immune cell migration across this brain barrier. Fluids Barriers CNS. 2016; 13: 2. https://doi.org/10.1186/s12987-016-0027-0 PMID: 26833402

35. Couderc T, Chrétien F, Schilte C, Disson O, Brigitte M, Guivel-Benhassine F, et al. A Mouse Model for Chikungunya: Young Age and Inefficient Type-I Interferon Signaling Are Risk Factors for Severe Disease. PLOS Pathog. 2008; 4: e29. https://doi.org/10.1371/journal.ppat.0040029 PMID: 18282093

36. Duan L, Zhang X-D, Miao W-Y, Sun Y-J, Xiong G, Wu Q, et al. PDGFRβ Cells Rapidly Relay Inflammatory Signal from the Circulatory System to Neurons via Chemokine CCL2. Neuron. 2018; 0. https://doi.org/10.1016/j.neuron.2018.08.030 PMID: 30269986

37. Gaceb A, Paul G. Pericyte Secretome. Adv Exp Med Biol. 2018; 1109: 139–163. https://doi.org/10.1007/978-3-030-02601-1_11 PMID: 30523595

38. Montagne A, Nikolakopoulou AM, Zhao Z, Sagare AP, Si G, Lazic D, et al. Pericyte degeneration causes white matter dysfunction in the mouse central nervous system. Nat Med. 2018; 24: 326–337. https://doi.org/10.1038/nm.4482 PMID: 29400711

39. Hartmann DA, Underly RG, Watson AN, Shih AY. A murine toolbox for imaging the neurovascular unit. Microcirc N Y N 1994. 2015; 22: 168–182. https://doi.org/10.1111/micc.12176 PMID: 25352367

40. Prasad VM, Miller AS, Klose T, Sirohi D, Buda G, Jiang W, et al. Structure of the immature Zika virus at 9 Å resolution. Nat Struct Mol Biol. 2017; 24: 184–186. https://doi.org/10.1038/nsmb.3352 PMID: 28067914

41. Hamel R, Dejarnac O, Wichit S, Ekchariyawat P, Neyret A, Luplertlop N, et al. Biology of Zika Virus Infection in Human Skin Cells. J Virol. 2015; 89: 8880–8896. https://doi.org/10.1128/JVI.00354-15 PMID: 26085147

42. Meertens L, Labeau A, Dejarnac O, Cipriani S, Sinigaglia L, Bonnet-Madin L, et al. Axl Mediates ZIKA Virus Entry in Human Glial Cells and Modulates Innate Immune Responses. Cell Rep. 2017; 18: 324–333. https://doi.org/10.1016/j.celrep.2016.12.045 PMID: 28076778

43. Nowakowski TJ, Pollen AA, Di Lullo E, Sandoval-Espinosa C, Bershteyn M, Kriegstein AR. Expression Analysis Highlights AXL as a Candidate Zika Virus Entry Receptor in Neural Stem Cells. Cell Stem Cell. 2016; 18: 591–596. https://doi.org/10.1016/j.stem.2016.03.012 PMID: 27038591

44. Richard AS, Shim B-S, Kwon Y-C, Zhang R, Otsuka Y, Schmitt K, et al. AXL-dependent infection of human fetal endothelial cells distinguishes Zika virus from other pathogenic flaviviruses. Proc Natl Acad Sci. 2017; 114: 2024–2029. https://doi.org/10.1073/pnas.1620558114 PMID: 28167751

45. Strange DP, Jiyarom B, Zarandi NP, Xie X, Baker C, Sadri-Ardekani H, et al. Axl Promotes Zika Virus Entry and Modulates the Antiviral State of Human Sertoli Cells. mBio. 2019; 10: e01372–19. https://doi.org/10.1128/mBio.01372-19 PMID: 31311882

46. Wells MF, Salick MR, Wiskow O, Ho DJ, Worringer KA, Ihry RJ, et al. Genetic Ablation of AXL Does Not Protect Human Neural Progenitor Cells and Cerebral Organoids from Zika Virus Infection. Cell Stem Cell. 2016; 19: 703–708. https://doi.org/10.1016/j.stem.2016.11.011 PMID: 27912091

47. Hastings AK, Yockey LJ, Jagger BW, Hwang J, Uraki R, Gaitsch HF, et al. TAM Receptors Are Not Required for Zika Virus Infection in Mice. Cell Rep. 2017; 19: 558–568. https://doi.org/10.1016/j.celrep.2017.03.058 PMID: 28423319

48. Dinner S, Borkowski J, Stump-Guthier C, Ishikawa H, Tenenbaum T, Schroten H, et al. A Choroid Plexus Epithelial Cell-based Model of the Human Blood-Cerebrospinal Fluid Barrier to Study Bacterial Infection from the Basolateral Side. JoVE J Vis Exp. 2016; e54061. https://doi.org/10.3791/54061 PMID: 27213495

49. Chiu CY, Martín CS-S, Bouquet J, Li T, Yagi S, Tamhankar M, et al. Experimental Zika Virus Inoculation in a New World Monkey Model Reproduces Key Features of the Human Infection. Sci Rep. 2017; 7: 17126. https://doi.org/10.1038/s41598-017-17067-w PMID: 29215081

50. Aid M, Abbink P, Larocca RA, Boyd M, Nityanandam R, Nanayakkara O, et al. Zika Virus Persistence in the Central Nervous System and Lymph Nodes of Rhesus Monkeys. Cell. 2017; 169: 610–620.e14. https://doi.org/10.1016/j.cell.2017.04.008 PMID: 28457610

51. Paz-Bailey G, Rosenberg ES, Doyle K, Munoz-Jordan J, Santiago GA, Klein L, et al. Persistence of Zika Virus in Body Fluids—Final Report. N Engl J Med. 2018; 379: 1234–1243. https://doi.org/10.1056/NEJMoa1613108 PMID: 28195756

52. Osuna CE, Lim S-Y, Deleage C, Griffin BD, Stein D, Schroeder LT, et al. Zika viral dynamics and shedding in rhesus and cynomolgus macaques. Nat Med. 2016; 22: 1448–1455. https://doi.org/10.1038/nm.4206 PMID: 27694931

53. Jurado KA, Yockey LJ, Wong PW, Lee S, Huttner AJ, Iwasaki A. Antiviral CD8 T cells induce Zika-virus-associated paralysis in mice. Nat Microbiol. 2018; 3: 141–147. https://doi.org/10.1038/s41564-017-0060-z PMID: 29158604

54. Bearer EL, Orci L. Endothelial fenestral diaphragms: a quick-freeze, deep-etch study. J Cell Biol. 1985; 100: 418–428. https://doi.org/10.1083/jcb.100.2.418 PMID: 3968170

55. Sarin H. Physiologic upper limits of pore size of different blood capillary types and another perspective on the dual pore theory of microvascular permeability. J Angiogenesis Res. 2010; 2: 14. https://doi.org/10.1186/2040-2384-2-14 PMID: 20701757

56. Johnson MB, Wang PP, Atabay KD, Murphy EA, Doan RN, Hecht JL, et al. Single-cell analysis reveals transcriptional heterogeneity of neural progenitors in human cortex. Nat Neurosci. 2015; 18: 637–646. https://doi.org/10.1038/nn.3980 PMID: 25734491

57. He L, Vanlandewijck M, Mäe MA, Andrae J, Ando K, Del Gaudio F, et al. Single-cell RNA sequencing of mouse brain and lung vascular and vessel-associated cell types. Sci Data. 2018; 5: 180160. https://doi.org/10.1038/sdata.2018.160 PMID: 30129931

58. Armulik A, Genové G, Mäe M, Nisancioglu MH, Wallgard E, Niaudet C, et al. Pericytes regulate the blood–brain barrier. Nature. 2010; 468: 557–561. https://doi.org/10.1038/nature09522 PMID: 20944627

59. Daneman R, Zhou L, Kebede AA, Barres BA. Pericytes are required for blood–brain barrier integrity during embryogenesis. Nature. 2010; 468: 562–566. https://doi.org/10.1038/nature09513 PMID: 20944625

60. Chang C-Y, Li J-R, Ou Y-C, Lin S-Y, Wang Y-Y, Chen W-Y, et al. Interplay of inflammatory gene expression in pericytes following Japanese encephalitis virus infection. Brain Behav Immun. 2017; 66: 230–243. https://doi.org/10.1016/j.bbi.2017.07.003 PMID: 28690034

61. Amara A, Mercer J. Viral apoptotic mimicry. Nat Rev Microbiol. 2015; 13: 461–469. https://doi.org/10.1038/nrmicro3469 PMID: 26052667

62. Chen J, Yang Y, Yang Y, Zou P, Chen J, He Y, et al. AXL promotes Zika virus infection in astrocytes by antagonizing type I interferon signalling. Nat Microbiol. 2018; 3: 302–309. https://doi.org/10.1038/s41564-017-0092-4 PMID: 29379210

63. Wilcox DR, Folmsbee SS, Muller WJ, Longnecker R. The Type I Interferon Response Determines Differences in Choroid Plexus Susceptibility between Newborns and Adults in Herpes Simplex Virus Encephalitis. mBio. 2016; 7: e00437–16, /mbio/7/2/e00437-16.atom. https://doi.org/10.1128/mBio.00437-16 PMID: 27073094

64. Gorman MJ, Caine EA, Zaitsev K, Begley MC, Weger-Lucarelli J, Uccellini MB, et al. An Immunocompetent Mouse Model of Zika Virus Infection. Cell Host Microbe. 2018; 23: 672–685.e6. https://doi.org/10.1016/j.chom.2018.04.003 PMID: 29746837

65. Liddelow SA, Dzięgielewska KM, Møllgård K, Whish SC, Noor NM, Wheaton BJ, et al. Cellular Specificity of the Blood–CSF Barrier for Albumin Transfer across the Choroid Plexus Epithelium. PLOS ONE. 2014; 9: e106592. https://doi.org/10.1371/journal.pone.0106592 PMID: 25211495

66. Grapp M, Wrede A, Schweizer M, Hüwel S, Galla H-J, Snaidero N, et al. Choroid plexus transcytosis and exosome shuttling deliver folate into brain parenchyma. Nat Commun. 2013; 4: 2123. https://doi.org/10.1038/ncomms3123 PMID: 23828504

67. O'Hara BA, Gee GV, Atwood WJ, Haley SA. Susceptibility of Primary Human Choroid Plexus Epithelial Cells and Meningeal Cells to Infection by JC Virus. J Virol. 2018; 92: e00105–18. https://doi.org/10.1128/JVI.00105-18 PMID: 29437972

68. Adcock RS, Chu Y-K, Golden JE, Chung D-H. Evaluation of anti-Zika virus activities of broad-spectrum antivirals and NIH clinical collection compounds using a cell-based, high-throughput screen assay. Antiviral Res. 2017; 138: 47–56. https://doi.org/10.1016/j.antiviral.2016.11.018 PMID: 27919709

69. Boroujerdi A, Tigges U, Welser-Alves JV, Milner R. Isolation and culture of primary pericytes from mouse brain. Methods Mol Biol Clifton NJ. 2014; 1135: 383–392. https://doi.org/10.1007/978-1-4939-0320-7_31 PMID: 24510880

70. Ishiwata I, Ishiwata C, Ishiwata E, Sato Y, Kiguchi K, Tachibana T, et al. Establishment and characterization of a human malignant choroids plexus papilloma cell line (HIBCPP). Hum Cell. 2005; 18: 67–72. https://doi.org/10.1111/j.1749-0774.2005.tb00059.x PMID: 16130902

71. Johnson DM, Sokoloski KJ, Jokinen JD, Pfeffer TL, Chu Y-K, Adcock RS, et al. Advanced Safety and Genetic Stability in Mice of a Novel DNA-Launched Venezuelan Equine Encephalitis Virus Vaccine with Rearranged Structural Genes. Vaccines. 2020; 8. https://doi.org/10.3390/vaccines8010114 PMID: 32121666

72. Wang F, Flanagan J, Su N, Wang L-C, Bui S, Nielson A, et al. RNAscope. J Mol Diagn. 2012; 14: 22–29. https://doi.org/10.1016/j.jmoldx.2011.08.002 PMID: 22166544

73. Bowyer JF, Thomas M, Patterson TA, George NI, Runnells JA, Levi MS. A Visual Description of the Dissection of the Cerebral Surface Vasculature and Associated Meninges and the Choroid Plexus from Rat Brain. J Vis Exp JoVE. 2012 [cited 21 May 2018]. https://doi.org/10.3791/4285 PMID: 23183685

74. Lanciotti Robert S., Kosoy Olga L., Laven Janeen J., Velez Jason O., Lambert Amy J., Johnson Alison J., et al. Genetic and Serologic Properties of Zika Virus Associated with an Epidemic, Yap State, Micronesia, 2007. Emerg Infect Dis J. 2008; 14: 1232. https://doi.org/10.3201/eid1408.080287 PMID: 18680646

75. Lim NK-H, Moestrup V, Zhang X, Wang W-A, Møller A, Huang F-D. An Improved Method for Collection of Cerebrospinal Fluid from Anesthetized Mice. JoVE J Vis Exp. 2018; e56774–e56774. https://doi.org/10.3791/56774 PMID: 29608146

76. Kowapradit J, Opanasopit P, Ngawhirunpat T, Apirakaramwong A, Rojanarata T, Ruktanonchai U, et al. In vitro Permeability Enhancement in Intestinal Epithelial Cells (Caco-2) Monolayer of Water Soluble Quaternary Ammonium Chitosan Derivatives. AAPS PharmSciTech. 2010; 11: 497–508. https://doi.org/10.1208/s12249-010-9399-7 PMID: 20333490